ORIGINAL ARTICLE

Journal of Neurochemistry | JNC | WILEY

Inactivation of seeding activity of amyloid β-protein aggregates in vitro

Hiroto Nakano[1] | Tsuyoshi Hamaguchi[1] | Tokuhei Ikeda[1,2] |
Takahiro Watanabe-Nakayama[3] | Kenjiro Ono[4] | Masahito Yamada[1,5]

[1]Department of Neurology and Neurobiology of Aging, Kanazawa University Graduate School of Medical Sciences, Kanazawa, Japan

[2]Department of Neurology, Ishikawa Prefectural Central Hospital, Kanazawa, Japan

[3]World Premier International Research Center Initiative (WPI)-Nano Life Science Institute, Kanazawa University, Kanazawa, Japan

[4]Division of Neurology, Department of Internal Medicine, Showa University, Tokyo, Japan

[5]Divition of Neurology, Department of Internal Medicine, Kudanzaka Hospital, Tokyo, Japan

Correspondence
Masahito Yamada, Department of Neurology and Neurobiology of Aging, Kanazawa University Graduate School of Medical Sciences, 13-1, Kanazawa 920-8640, Japan.
E-mail: m-yamada@med.kanazawa-u.ac.jp

Funding information
Japan Society for the Promotion of Science, Grant/Award Number: JP20K07863 and JP17H04194

Abstract

The deposition of amyloid beta-protein (Aβ) in the brain is a major pathological feature of Alzheimer's disease (AD). Recent studies have reported that Aβ pathology can be transmitted among individuals through medical procedures in humans, as well as animal models, and the prevention of Aβ pathology transmission is of great importance to public health. To assess the effect of autoclaving (AC) or gamma (γ)-ray irradiation on Aβ pathology transmission, we evaluated the seeding effect of Aβ aggregates using thioflavin T (ThT) assays and high-speed atomic force microscopy (HS-AFM) and investigated the structural changes in the Aβ aggregates after treatment with AC or γ-ray irradiation using ThT assays, circular dichroism (CD) spectroscopy, and electron microscopy (EM). The ThT assays and HS-AFM showed that the seeding effect of Aβ aggregates was inactivated by AC at different temperatures, exposure times, and concentrations of Aβ aggregates during treatment with AC. The results of the ThT fluorescence and CD spectral patterns of the autoclaved Aβ aggregates indicate that AC reduced β-sheet-rich structures in Aβ aggregates. The EM images demonstrated that the length of the autoclaved Aβ aggregates with fibril-like structures was significantly shorter than that of the untreated ones. Gamma-ray irradiation of Aβ aggregates did not lead to significant inactivation of the Aβ seeding effect or cause structural changes in Aβ aggregates. In conclusion, autoclaving Aβ aggregates decreases β-sheet-rich structures and reduces Aβ seeding activity, which could lead to the development of effective methods for preventing the propagation of Aβ pathology among individuals.

KEYWORDS
aggregation, Alzheimer's disease, autoclaving, propagation, seeding effect, γ-ray irradiation

1 | INTRODUCTION

Neurodegenerative diseases, including Alzheimer's disease (AD), Parkinson's disease (PD), dementia with Lewy bodies (DLB), amyotrophic lateral sclerosis (ALS), and prion diseases, have similar pathological features such as accumulation of misfolded proteins in the brain (Kushwah et al., 2020; Thomzig et al., 2014). Misfolded proteins, such as amyloid beta-protein (Aβ) and tau protein in AD, alpha (α)-synuclein in PD and DLB, transactive response DNA-binding protein of 43 kDa in ALS, and prion protein (PrP) in prion diseases, are associated with their corresponding disease pathogenesis. Conformational changes in these proteins from their native states to pathogenic states are associated with irreversible damage to the central nervous system, leading to various neurological symptoms (Soto et al., 2018).

Aβ is the main component of senile plaques, which are the major pathological features of AD and consists of 37–43 amino acids (Tiwari et al., 2019; Watts et al., 2018). The most common forms of Aβ are Aβ1-40 (Aβ40) and Aβ1-42 (Aβ42). Aβ42 is highly neurotoxic and can easily form Aβ42 aggregates (Srivastava et al., 2019; Tiwari et al., 2019). The Aβ aggregation is based on "nucleation-dependent polymerization models," and Aβ generates fibrillar structures through polymers, including low-molecular-weight oligomers, high-molecular-weight oligomers, and protofibrils (Chatani et al., 2018; Hoshino, 2017; Ono et al., 2020; Penke et al., 2017). During Aβ aggregation, secondary structures transited from random coil structures to β-sheets via α-helices were observed, and different types of secondary structures of Aβ aggregates show different spectral patterns in circular dichroism (CD) spectroscopy (Ono et al., 2010, 2013). Among the polymers, oligomeric and protofibril species of Aβ aggregates are more cytotoxic than fully mature fibrils (Kotler et al., 2014; Matsumura et al., 2011; Nguyen & Derreumaux, 2020; Nguyen et al., 2021; Sahoo et al., 2020; Said et al., 2020). Molecular analysis of the interaction between Aβ oligomers and the cell membrane is of great importance to reveal the biological features of Aβ oligomer neurotoxicity. Previous reports demonstrated that the interaction of Aβ oligomers and ganglioside-containing cell membranes developed structural conversions from α-helices to β-sheets in Aβ aggregates (Cheng et al., 2020; Rudajev et al., 2020). However, the precise pathomechanisms of neuronal damage caused by Aβ oligomers remain uncertain because of their transient and heterogeneous properties (Cawood et al., 2021; Nguyen et al., 2020).

Previous studies indicated that misfolded proteins are transmissible among individuals as a behavior of PrP (Jucker et al., 2018; Yamada et al., 2019). Aβ has been reported to self-propagate, and numerous studies have shown that Aβ pathology can propagate among individuals under experimental settings using mouse models (Burwinkel et al., 2018; Hamaguchi et al., 2012; Jucker et al., 2018; Langer et al., 2011; Meyer-Luehmann et al., 2006; Watts et al., 2011). In clinical situations, pathological studies of autopsied patients with iatrogenic Creutzfeldt-Jakob disease indicated that Aβ pathology in the brain might be transmitted among humans via medical procedures, such as human cadaveric dura mater grafting and human cadaveric pituitary-derived growth hormone injections (Cali et al., 2018; Duyckaerts et al., 2018; Frontzek et al., 2016; Hamaguchi et al., 2016; Jaunmuktane et al., 2015; Kovacs

et al., 2016; Preusser et al., 2006; Purro et al., 2018; Ritchie et al., 2017; Simpson et al., 1996). Several studies have shown that transmission of Aβ pathology via dura mater grafts or neurosurgical instruments can cause symptomatic Aβ-cerebral amyloid angiopathy-related hemorrhages after incubation periods of 25 years or longer (Banerjee et al., 2019; Ehling et al., 2012; Hamaguchi et al., 2019; Hervé et al., 2018; Jaunmuktane et al., 2018; Nakayama et al., 2017; Purrucker et al., 2013; Raposo et al., 2020; Yamada et al., 2019; Yoshiki et al., 2021). Therefore, the development of inactivation methods for Aβ seeding activity is critical to prevent iatrogenic transmission of Aβ pathology.

Several sterilization treatments, such as autoclaving (AC), hydrogen peroxide gas plasma sterilization, and gamma (γ)-ray irradiation, have been widely used for the sterilization of surgical devices (Harrell et al., 2018; Yoo, 2018). The effectiveness of formic acid sterilization, formaldehyde fixation, boiling, and hydrogen peroxide gas plasma sterilization in preventing the propagation of Aβ pathology have been analyzed (Eisele et al., 2009; Fritschi et al., 2014; Meyer-Luehmann et al., 2006). Application of 70% formic acid for 1 h or plasma sterilization using a STERRAD 100 S hydrogen peroxide gas plasma sterilizer diminished Aβ seeding activity under experimental conditions in transgenic AD mouse models (Eisele et al., 2009; Meyer-Luehmann et al., 2006). Although formic acid sterilization is not commonly preferred because of its hazardous and toxic properties (Pietzke et al., 2020), hydrogen peroxide gas plasma sterilization is widely used for neurosurgical devices.

Previous reports have demonstrated that AC was effective in inactivating PrP transmission, and combination methods of AC with chemical detergents, such as sodium hydroxide (NaOH), alkaline detergent, and sodium dodecyl sulfate (SDS), are recommended for sterilizing devices used on patients with prion diseases (Fichet et al., 2004, 2007). A recent study reported that the seeding activity of α-synuclein was also inactivated by AC in animal experiments (Tarutani et al., 2018). However, no studies have elucidated the underlying molecular mechanisms of the sterilization method.

To establish other methods for inactivating Aβ seeding activities and reveal its underlying molecular mechanisms, the changes in Aβ seeding activities and steric structures of Aβ aggregates after treatment with the AC or γ-ray irradiation sterilization methods were examined. In this study, thioflavin T (ThT) assays and high-speed atomic force microscopy (HS-AFM) were performed to evaluate Aβ seeding activities. In addition, ThT assays, CD spectroscopy, and electron microscopy (EM) were used to investigate the structural features of Aβ aggregates.

2 | MATERIALS AND METHODS

The study was not pre-registered.

2.1 | Ethical statement

No animal was used in this study. We confirm that institutional ethical approval was not required for this study.

NAKANO ET AL.

Journal of Neurochemistry | JNC | The Official Journal of the International Society for Neurochemistry | WILEY | **501**

2.2 | Preparation of Aβ samples

Synthetic Aβ40 (cat.no. 4307-v) and Aβ42 (cat.no. 4349-v) peptide lyophilizates (a trifluoroacetate form, purity ≥ 95.0% evaluated using high-performance liquid chromatography) were purchased from a chemical facility (Peptide Institute, Inc.). The peptide lyophilizates were stored at −80°C until use. The Aβ peptide lyophilizates were dissolved at a concentration of 25 μM in mixed buffers containing 10% (v/v) of 0.02% ammonia solution and 90% (v/v) of 10 mM phosphate buffer (pH 7.4) and sonicated for 1 min using an ultrasonic disruptor, UD-201 (TOMY SEIKO Co., Ltd.). Sonicated Aβ solutions were immediately frozen in liquid nitrogen and stored at −80°C until use. The frozen samples were thawed and centrifuged at 16 000 g at 4°C for 10 min using a centrifugal machine, MX-300 (TOMY SEIKO Co., Ltd.). We used the supernatant of the samples (non-aggregated Aβ40 and Aβ42). We defined the Aβ concentrations of each sample using the concentrations of Aβ at the dissolution process of Aβ peptides, as previously reported (Ono et al., 2012).

To prepare Aβ aggregates, non-aggregated Aβ40 and Aβ42 were incubated at 37°C for 10 days (Aβ40) (untreated Aβ40 aggregates) or 2 days (Aβ42) (untreated Aβ42 aggregates). The Aβ aggregates in this study contain multiple compounds, including Aβ fibrils (fAβ), protofibrils, and oligomers, because these components would be in equilibrium, as previously reported (Lu et al., 2013; Roychaudhuri et al., 2009). Each sample was stored at −80°C until use.

2.3 | AC procedure of untreated Aβ aggregates

A 500 μl aliquot of untreated Aβ40 and Aβ42 aggregates was poured into Myghty vials (Maruemu Corp., cat.no. 5-115-01). These samples were incubated in a gravity displacement-type AC, LSX-300 (TOMY SEIKO Co., Ltd.), under the following conditions: temperature: 105, 110, 115, and 120°C (Aβ40); 105, 110, 115, 120, 125, 130, and 135°C (Aβ42); exposure times: 5, 15, 30, and 60 min (Aβ40), and 5, 15, 30, 60, 90, and 120 min (Aβ42). After the AC procedures, each sample was immediately put on ice and stored at −80°C until use (autoclaved Aβ aggregates).

2.4 | Gamma-ray irradiation of untreated Aβ aggregates

A 500 μl aliquot of untreated Aβ40 and Aβ42 aggregates was poured into Protein Lobind tubes (Eppendolf Japan Co., Ltd., cat. no. 0030108116) and sent to a sterilization facility (Koga Isotope, Ltd.) under cold conditions (−15°C). These samples were irradiated with γ-rays (25 or 50 kGy). After the treatments, these samples were sent back to our laboratory under cold conditions (−15°C) and stored at −80°C until use (Aβ aggregates with γ-ray irradiation).

2.5 | Monitoring of temporal changes in the ThT fluorescence of Aβ assembly containing non-aggregated Aβ and Aβ aggregates with different treatments

To evaluate the seeding activities of different types of Aβ aggregates (untreated Aβ aggregates, autoclaved Aβ aggregates, and Aβ aggregates with γ-ray irradiation), we monitored temporal changes in the Aβ aggregates quantities in mixed samples containing Aβ aggregates and non-aggregated Aβ by ThT assays. We thawed untreated Aβ aggregates, autoclaved Aβ aggregates, and Aβ aggregates with γ-ray irradiation. Each sample was sonicated on ice for 30 s using an ultrasonic disruptor. Sonicated Aβ aggregates were added to non-aggregated Aβ solutions at a ratio of 1:9 (v/v). After brief vortexing, the mixed samples were incubated at 37°C for 7 days (Aβ40) (Aβ40 assembly) or 12 h (Aβ42) (Aβ42 assembly). Non-aggregated Aβ without Aβ aggregates were also incubated at 37°C for 7 days (Aβ40) (Aβ40 assembly) or 12 h (Aβ42) (Aβ42 assembly).

To perform the ThT assays, we prepared 5 μM ThT solutions (Wako Pure Chemical Industries, Ltd., cat.no. 02-01002). ThT has been used for quantitative studies of Aβ aggregates by binding to β-sheet-rich structures in Aβ aggregates (Biancalana et al., 2010). ThT was dissolved in mixed buffers containing 10% (v/v) of 50 mM glycine-NaOH buffer (pH 8.5) and 90% (v/v) of double distilled water (DDW). We prepared mixed buffers containing 1 ml of ThT solution and 3 μl of Aβ samples (Aβ40 and Aβ42 assemblies), and the ThT fluorescence of the mixed buffers was measured three times using a Hitachi F-7000 fluorometer (Hitachi High-Tech Science Corp.). Excitation and emission wavelengths of 450 nm and 482 nm were used for this assay. Fluorescence was determined by the mean of four measurements by subtraction of the ThT blank readings. The ThT fluorescence of Aβ aggregates would increase unless the ThT fluorescence of sample buffers was not subtracted from the raw ThT fluorescence of Aβ samples. The seeding activity of Aβ aggregates was analyzed using a 50% seeding dose (SD_{50}), which was defined as the time at 50% of the peak value of Aβ aggregates in the seeding assays. Shorter times of SD_{50} in the seeding assays indicated a higher seeding activity of Aβ aggregates in this study. To calculate SD_{50} in the seeding assays, sigmoidal curve fittings of the ThT fluorescence data were performed using Igor Pro version 8 software (HULINKS Inc.).

Another ThT assay using Aβ aggregates treated with AC at different concentrations of Aβ aggregates was performed to evaluate the seeding activity of autoclaved Aβ aggregates treated at different concentrations. Untreated Aβ aggregates at a concentration of 25 μM were diluted in 10 mM phosphate buffer (pH 7.4) at the concentrations of 0.25 μM and 2.5 μM. To prepare untreated Aβ aggregates at a concentration of 250 μM, the Aβ peptide lyophilizates were dissolved at a concentration of 250 μM in mixed buffer containing 10% (v/v) of 0.02% ammonia solution and 90% (v/v) of 10 mM phosphate buffer (pH 7.4) and incubated for 10 days (Aβ40) (untreated Aβ40 aggregates) or 2 days (Aβ42) (untreated Aβ42 aggregates) with agitation at 37°C.

A 500 µl aliquot of each Aβ aggregate sample at different concentrations (0.25, 2.5, 25, and 250 µM) was poured into glass bottles. These samples were autoclaved at 105°C for 5 min (Aβ40) or 120°C for 30 min (Aβ42). After the AC procedures, these samples were diluted in 10 mM phosphate buffer at a concentration of 0.25 µM for the Aβ aggregates. The samples were sonicated for 30 s, and a 500 µl aliquot of each sonicated Aβ aggregate sample (0.25 µM) was incubated with 45 µl of non-aggregated Aβ (25 µM) (final concentrations: non-aggregated Aβ: 2.1 µM, Aβ aggregates: 0.23 µM). This procedure meant that the concentrations of Aβ aggregates, which were added to non-aggregated Aβ, were same in all Aβ assemblies in both Aβ40 and Aβ42. These mixed samples were incubated at 37°C for 9 days (Aβ40) (Aβ40 assembly) or 2 days (Aβ42) (Aβ42 assembly). We prepared 10 µM ThT solutions containing 10% (v/v) of 50 mM glycine-NaOH buffer (pH 8.5) and 90% (v/v) of DDW. We prepared mixed buffers containing 1 ml of ThT solution (10 µM) and 5 µl of Aβ samples (Aβ40 and Aβ42 assemblies). The ThT fluorescence of the mixed buffers was measured four times using a Hitachi F-7000 fluorometer. The seeding activity of Aβ aggregates was analyzed using the SD_{50}.

2.6 | Video imaging of elongation of Aβ42 aggregates with HS-AFM

The Aβ42 peptide lyophilizates were diluted at a concentration of 200 µM in mixed buffers containing 10% (v/v) of 0.02% ammonia solution and 90% (v/v) of 10 mM phosphate buffer (pH 7.4). To remove large Aβ42 aggregates, which would interrupt the observation of small Aβ42 aggregates in HS-AFM, the solution was poured into Amicon Ultrafiltration devices (30 K) (Merck Co., Ltd., cat. no. UFC503096), and centrifuged at 14 000 g at 4°C for 15 min. After measuring the Aβ42 concentration in the filtrate using a V-650 ultraviolet-visible spectrophotometer (JASCO), the sample was stored at −80°C until use (Aβ42 with filtration). A 500 µl aliquot of untreated Aβ42 aggregates at a concentration of 25 µM was autoclaved at 120°C for 30 min or 135°C for 120 min, and these samples were stored at −80°C until use (autoclaved Aβ42 aggregates). We reconstituted untreated and autoclaved Aβ42 aggregates as well as Aβ42 with filtration at 5 µM in 10 mM phosphate buffer (pH 7.4) containing 100 mM NaCl.

A sample–scanning type of HS-AFM was operated in the amplitude modulation–tapping mode with a BL-AC10DS-A2 cantilever (Olympus Corp.) (Ando et al., 2001; Sahoo et al., 2019; Uchihashi et al., 2012; Watanabe-Nakayama et al., 2016, 2020). The cantilever probes were prepared at the top of the cantilevers by electron-beam deposition using the scanning electron microscope mode of ELS-7500, which is an electron lithography system (Elionix Inc.). The operation methods of HS-AFM were based on a previous report (Watanabe-Nakayama et al., 2016, 2020). Before the injection of Aβ42 with filtration into the sample chamber of HS-AFM, a 2 µl aliquot of each Aβ42 aggregate sample (untreated Aβ42 aggregates and autoclaved Aβ42 aggregates treated at 120°C for 30 min or 135°C for 120 min) was spotted onto mica to attach the Aβ42 aggregates. Each sample was incubated on mica at room temperature (RT) (22°C) for 20 min. After incubation, the mica was washed out using 20 µl of 10 mM phosphate buffer (pH 7.4) containing 100 mM NaCl, and Aβ42 aggregates were observed using HS-AFM. The frame rates of the four different groups of HS-AFM images were 0.1 frames per second, and the pixel sizes were 400 × 400. Aβ42 with filtration at a concentration of 5 µM containing 100 mM NaCl was used as the buffer in the sample chamber of HS-AFM.

We monitored the elongation of Aβ42 aggregates in four different groups (Aβ42 with filtration incubated with untreated Aβ42 aggregates, autoclaved Aβ42 aggregates treated at 120°C for 30 min, autoclaved Aβ42 aggregates treated at 135°C for 120 min, or no Aβ42 aggregates). All four groups were examined three times, and HS-AFM images were captured every 10 s. The number of Aβ42 aggregates was counted every 100 s. The length of all Aβ42 aggregates was measured by subtracting the initial length from the final length of the Aβ42 aggregates. The total elongation period of each Aβ42 aggregate was measured. The elongation speed of the Aβ42 aggregates was also calculated.

2.7 | Evaluation of ThT fluorescence in Aβ aggregates after treatment with AC or γ-ray irradiation

To evaluate the structural changes in Aβ aggregates after treatment with AC or γ-ray irradiation, we performed ThT assays using different types of Aβ aggregates. We prepared three different types of Aβ40 and Aβ42 aggregates as follows: untreated Aβ aggregates, autoclaved Aβ aggregates (120°C for 5 min: Aβ40 or 135°C for 120 min: Aβ42), and Aβ aggregates with γ-ray irradiation at 50 kGy. It took approximately 1 h for the Aβ40 aggregates to perform AC at 120°C for 5 min in glass bottles. A 500 µl aliquot of each sample (untreated Aβ40 aggregates and Aβ40 aggregates with γ-ray irradiation at 50 kGy) was poured into glass bottles, and incubated at RT (22°C) for 1 h to make sample conditions equal among the different Aβ40 aggregates samples (untreated Aβ40 aggregates, autoclaved Aβ40 aggregates treated at 120°C for 5 min, and Aβ40 aggregates with γ-ray irradiation at 50 kGy) except for treatment (AC or γ-ray irradiation). It took approximately 4 h for Aβ42 aggregates to perform AC at 135°C for 120 min in glass bottles. A 500 µl aliquot of each sample (untreated Aβ42 aggregates, and Aβ42 aggregates with γ-ray irradiation at 50 kGy) was poured into glass bottles, and we incubated these samples at RT (22°C) for 4 h to ensure equal sample conditions among them (untreated Aβ42 aggregates, autoclaved Aβ42 aggregates treated at 135°C for 120 min, and Aβ42 aggregates with γ-ray irradiation at 50 kGy), except for treatment (AC or γ-ray irradiation). A 500 µl aliquot of 10 mM phosphate buffer was also poured into glass bottles and incubated at RT (22°C) for 1 or 4 h as control samples. ThT fluorescence of each sample was examined using the same seeding assay protocol described above.

2.8 | Measurement of spectral patterns of Aβ aggregates in CD spectroscopy

We examined the CD spectral patterns of different types of Aβ aggregates to study the structural changes in Aβ aggregates after treatment (AC or γ-ray irradiation). A 200 µl aliquot of non-aggregated Aβ, untreated Aβ aggregates, and autoclaved Aβ aggregates treated under the following conditions: temperatures: 105, 110, 115, and 120°C (Aβ40); 120, 125, 130, and 135°C (Aβ42); exposure times: 5, 15, 30, and 60 min (Aβ40), and 30, 60, 90, and 120 min (Aβ42), and Aβ aggregates with γ-ray irradiation (25 or 50 kGy) were placed into a CD cuvette with a path length of 1 mm (Hellma, cat.no. 100-1-20). Spectrum signals of Aβ aggregates were recorded from 185 to 250 nm at a 0.1-nm resolution with a scan rate of 50 nm/min using a J-805 spectropolarimeter (JASCO). Ten scans were performed, and raw datasets were manipulated by smoothing and subtracting the buffer spectra according to the manufacturer's instructions. The datasets were converted to molar ellipticity ($kdeg \cdot cm^2/dmol$).

2.9 | EM images of Aβ aggregates with fibril-like structures

We evaluated the structural features of Aβ aggregates with fibril-like structures between untreated and autoclaved Aβ aggregates. Each untreated and autoclaved Aβ aggregate sample (120°C for 5 min: Aβ40, 135°C for 120 min: Aβ42) was diluted two-fold in 10 mM phosphate buffer (pH 7.4). A 20 µl aliquot of each sample was spotted onto glow-discharged, carbon-coated formvar grids (Okenshoji Co., Ltd., cat.no. 10-1009) and incubated for 20 min. The droplets were displaced by an equal volume of 2.5% (v/v) glutaraldehyde solution (Wako Pure Chemical Industries Ltd., cat.no. 073-00536) and incubated for an additional 4 min. The grids were stained with 15 µl of 1% (v/v) uranyl acetate dihydrate (Wako Pure Chemical Industries Ltd., cat.no. 94260). These solutions were removed, and the grids were air-dried. The EM images were examined using a Hitachi H-7650 (Hitachi High-Tech Science Corp.). We randomly selected 30 fibers of Aβ aggregates with fibril-like structures, and the width and length of Aβ aggregates with fibril-like structures were measured. The magnification of the EM images was 30 000× when we measured the width of Aβ aggregates with fibril-like structures and 5000–30 000× when we measured the length of Aβ aggregates with fibril-like structures.

2.10 | Statistical analysis

Neither inclusion nor exclusion criteria were pre-determined in this study. Prior to statistical analysis, datasets were assessed for normality using a D'Agostino and Pearson test in the GraphPad Prism software (version 8.0.2; MDF Co., Ltd.). Unfortunately, we could not check the normality of data of SD_{50} and ThT fluorescence in the ThT assays because of the insufficient numbers of data. A one-way factorial ANOVA followed by Dunnett's post hoc comparisons was used to evaluate statistical significance in SD_{50} among non-aggregated Aβ and each Aβ aggregates (untreated Aβ aggregates, autoclaved Aβ aggregates treated with different conditions of AC at different temperatures or different exposure times and Aβ aggregates with γ-ray irradiation) in the evaluation of seeding activities of Aβ aggregates after different treatments using ThT assays. A one-way factorial ANOVA followed by Tukey post hoc comparisons was used to evaluate statistical significance in SD_{50} among non-aggregated Aβ and each Aβ aggregate (untreated Aβ aggregates and autoclaved Aβ aggregates treated at different concentrations) in the evaluation of the seeding activities of Aβ aggregates after AC at different concentrations using ThT assays. The statistical significance of the ThT fluorescence among the samples (10 mM phosphate buffer, untreated Aβ aggregates, autoclaved Aβ aggregates, and Aβ aggregates with γ-ray irradiation at 50 kGy) was also evaluated using a one-way factorial ANOVA followed by Tukey post hoc comparisons. These tests were performed using a GraphPad Prism software (version 8.0.2).

The results of both the elongation speed of Aβ42 aggregates in HS-AFM and the length of Aβ aggregates with fibril-like structures in EM images were not normally distributed, and we used Brunner–Munzel tests to evaluate the statistical significance of the HS-AFM datasets without assuming normal distribution and equal variance, as previously reported (Watanabe-Nakayama et al., 2016, 2020). These tests were performed using a R software version 3.6.2. The length of Aβ aggregates with fibril-like structures in EM images was evaluated using a Mann–Whitney U test using a GraphPad Prism software. The width of Aβ aggregates with fibril-like structures in EM images was evaluated using a t-test based on the normal distribution of data. We described the statistical data in the manuscript using the following terms: *P-value* (*p*), *F-value* (*f*), *T-value* (*t*), and *degrees of freedom* (*df*). The level of significance was set at $p < 0.05$.

The temporal changes in the ThT fluorescence of the Aβ assemblies containing non-aggregated Aβ and Aβ aggregates treated with different agents are presented as mean values, while the error bars indicate standard deviations (SD) (Figures 1 and 2). All data of the SD_{50} in the ThT assays are plotted in the bar graphs showing the mean values of the SD_{50}, while the error bars indicate SD (Figures 1 and 2). The temporal changes in the cumulative number of Aβ42 aggregates during the observation of the elongation of Aβ42 aggregates using HS-AFM are presented as real numbers (Figure 3e), while the elongation speed of the Aβ42 aggregates during the observation of the elongation of Aβ42 aggregates using HS-AFM are presented as median values in the box-and-whisker plot (Figure 3f). All data of the ThT fluorescence in the ThT assays are plotted in the bar graphs showing the mean values of the ThT fluorescence, while the error bars indicate SD (Figure 4). Spectral curves of Aβ aggregates in CD spectroscopy are presented as the mean values of the spectrum signals of Aβ aggregates (Figure 5). All data of the width and length of Aβ aggregates with fibril-like structures in EM images are plotted in the bar graphs showing the mean values of each measurement, while the error bars indicate SD (Figure 6e, f). No randomization was performed to allocate subjects in this study. Blinding was not performed and test for outliers was not conducted. In this study, no
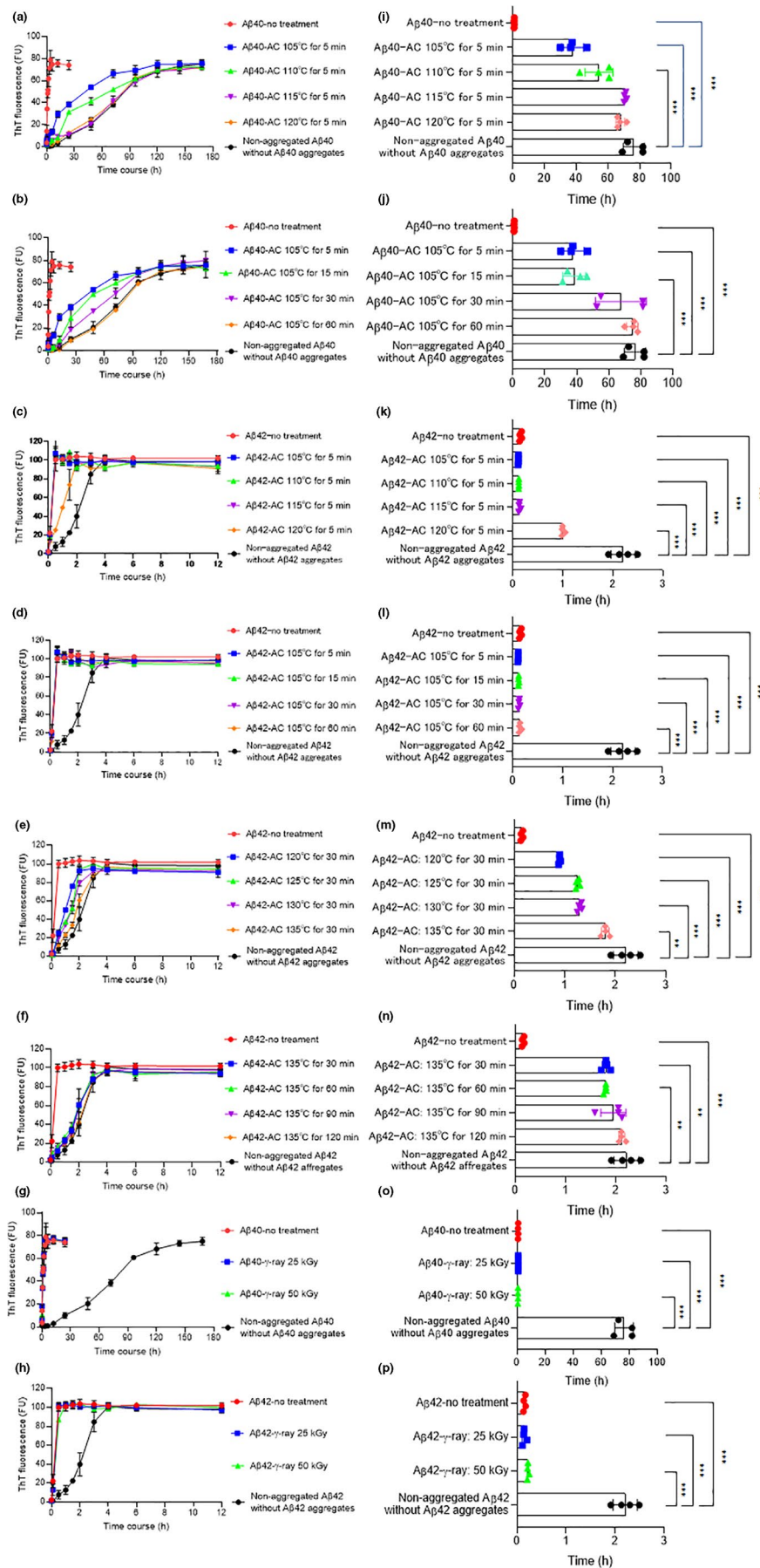
FIGURE 1 Temporal changes in the thioflavin T (ThT) fluorescence of amyloid beta-protein (Aβ) assemblies containing non-aggregated Aβ and Aβ aggregates treated with different agents. The temporal changes in the ThT fluorescence (a–h) and 50% seeding dose (SD_{50}) (i–p) of six different types of Aβ1-40 (Aβ40) and Aβ1-42 (Aβ42) assemblies are shown as follows: (a) and (i), 1. Non-aggregated Aβ40 and Aβ40 aggregates without AC (Aβ40-no treatment); 2–5. Non-aggregated Aβ40 and autoclaved Aβ40 aggregates treated at 105°C for 5 min (Aβ40-AC 105°C for 5 min), 110°C for 5 min (Aβ40-AC 110°C for 5 min), 115°C for 5 min (Aβ40-AC 115°C for 5 min), and 120°C for 5 min (Aβ40-AC 120°C for 5 min); and 6. Non-aggregated Aβ40 without Aβ40 aggregates; (b) and (j), 1. Aβ40-no treatment; 2–5. Non-aggregated Aβ40 and autoclaved Aβ40 aggregates treated at 105°C for 5 min (Aβ40-AC 105°C for 5 min), 105°C for 15 min (Aβ40-AC 105°C for 15 min), 105°C for 30 min (Aβ40-AC 105°C for 30 min), and 105°C for 60 min (Aβ40-AC 105°C for 60 min); and 6. Non-aggregated Aβ40 without Aβ40 aggregates; (c) and (k), 1. Non-aggregated Aβ42 and Aβ42 aggregates without AC (Aβ42-no treatment); 2–5. Non-aggregated Aβ42 and autoclaved Aβ42 aggregates treated at 105°C for 5 min (Aβ42-AC 105°C for 5 min), 110°C for 5 min (Aβ42-AC 110°C for for 5 min), 115°C for 5 min (Aβ42-AC 115°C for 5 min), and 120°C for 5 min (Aβ42-AC 120°C for 5 min); and 6. Non-aggregated Aβ42 without Aβ42 aggregates; (d) and (l), 1. Aβ42-no treatment; 2–5. Non-aggregated Aβ42 and autoclaved Aβ42 aggregates treated at 105°C for 5 min (Aβ42-AC 105°C for 5 min), 105°C for 15 min (Aβ42-AC 105°C for 15 min), 105°C for 30 min (Aβ42-AC 105°C for 30 min), and 105°C for 60 min (Aβ42-AC 105°C for 60 min); and 6. Non-aggregated Aβ42 without Aβ42 aggregates; (e) and (m), 1. Aβ42-no treatment; 2–5. Non-aggregated Aβ42 and autoclaved Aβ42 aggregates treated at 120°C for 30 min (Aβ42-AC 120°C for 30 min), 125°C for 30 min (Aβ42-AC 125°C for 30 min), 130°C for 30 min (Aβ42-AC 130°C for 30 min), and 135°C for 30 min (Aβ42-AC 135°C for 30 min); and 6. Non-aggregated Aβ42 without Aβ42 aggregates; (f) and (n), 1. Aβ42-no treatment; 2–5. Non-aggregated Aβ42 and autoclaved Aβ42 aggregates treated at 135°C for 30 min (Aβ42-AC 135°C for 30 min), 135°C for 60 min (Aβ42-AC 135°C for 60 min), 135°C for 90 min (Aβ42-AC 135°C for 90 min), and 135°C for 120 min (Aβ42-AC 135°C for 120 min); and 6. Non-aggregated Aβ42 without Aβ42 aggregates; (g) and (o), 1. Aβ40-no treatment; 2, 3. Non-aggregated Aβ40 and Aβ40 aggregates with γ-ray irradiation at 25 kGy (Aβ40-γ-ray 25 kGy) and 50 kGy (Aβ40-γ-ray 50 kGy); and 4. Non-aggregated Aβ40 without Aβ40 aggregates; (h) and (p), 1. Aβ42-no treatment; 2, 3. Non-aggregated Aβ42 and Aβ42 aggregates with γ-ray irradiation at 25 kGy (Aβ42-γ-ray 25 kGy) and 50 kGy (Aβ42-γ-ray 50 kGy); and 4. Non-aggregated Aβ42 without Aβ42 aggregates. Average values of four ThT fluorescence measurements in each Aβ assembly are plotted with error bars indicating standard deviations (SD) (a–h). Four datasets of SD_{50} in each Aβ assembly are plotted in bar graphs indicating the mean values of SD_{50}, while the error bars indicate SD (i–p). Asterisks indicate statistical significance between the two groups indicated by brackets (*$p < 0.05$, **$p < 0.01$, ***$p < 0.001$) (one-way ANOVA with Dunnett's post hoc comparison)
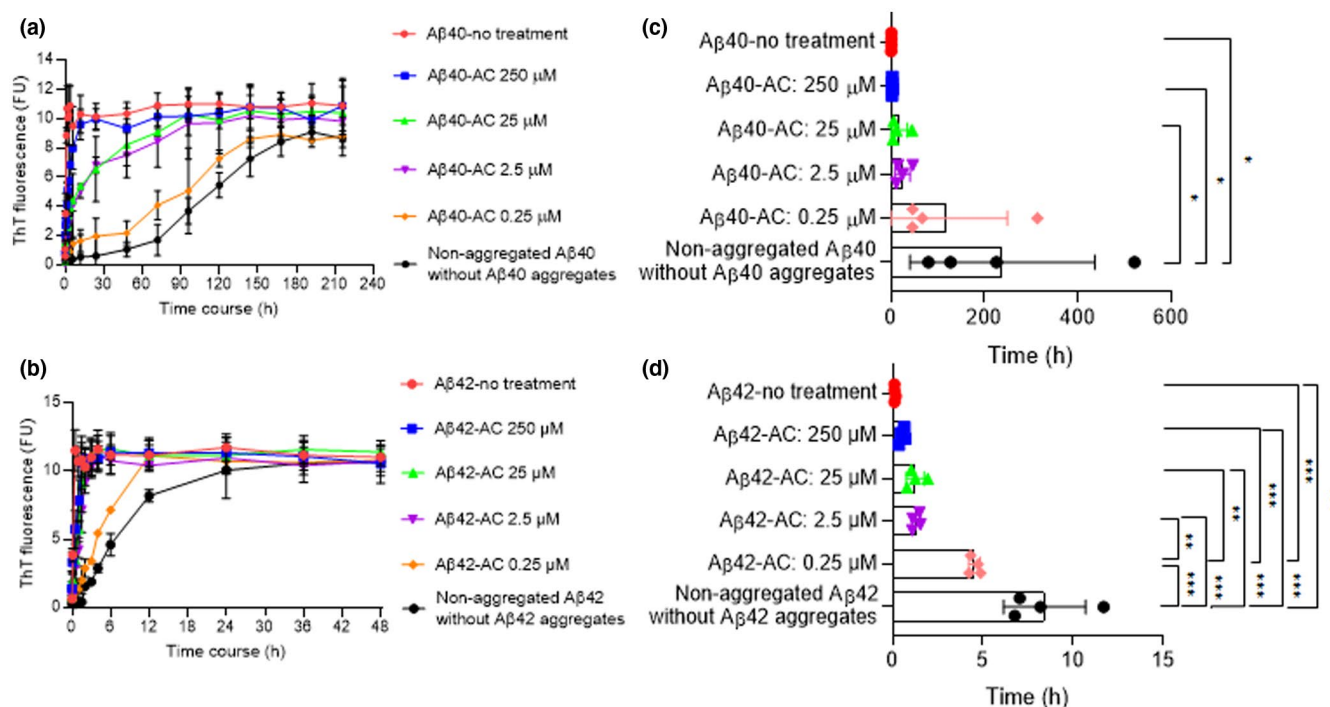

**FIGURE 2** Temporal changes in the thioflavin T (ThT) fluorescence of amyloid beta-protein (Aβ) assemblies containing non-aggregated Aβ and Aβ aggregates autoclaved at different concentrations. We show the temporal changes in the ThT fluorescence (a and b) and 50% seeding dose (SD_{50}) (c and d) of six different types of Aβ1-40 (Aβ40) assemblies and Aβ1-42 (Aβ42) assemblies as follows: (a) and (c), 1. Non-aggregated Aβ40 and Aβ40 aggregates without AC (Aβ40-no treatment); 2–5. Non-aggregated Aβ40 and autoclaved Aβ40 aggregates treated at a concentration of 250 μM (Aβ40-AC 250 μM), 25 μM (Aβ40-AC 25 μM), 2.5 μM (Aβ40-AC 2.5 μM), and 0.25 μM (Aβ40-AC 0.25 μM); and 6. Non-aggregated Aβ40 without Aβ40 aggregates; (b) and (d), 1. Non-aggregated Aβ42 and Aβ42 aggregates without AC (Aβ42-no treatment); 2–5. Non-aggregated Aβ42 and autoclaved Aβ42 aggregates treated at a concentration of 250 μM (Aβ42-AC 250 μM), 25 μM (Aβ42-AC 25 μM), 2.5 μM (Aβ42-AC 2.5 μM), and 0.25 μM (Aβ42-AC 0.25 μM); and 6. Non-aggregated Aβ42 without Aβ42 aggregates. Average values of four ThT fluorescence measurements in each Aβ assembly are plotted with errar bars indicating standard deviations (SD) (a and b). Four datasets of SD_{50} in each Aβ assembly are plotted in bar graphs indicating mean values of SD_{50}, while the error bars indicate SD (c and d). Asterisks indicate statistical significance between the two groups indicated by brackets (*$p < 0.05$, **$p < 0.01$, ***$p < 0.001$) (one-way ANOVA with Tukey post hoc comparisons)

(a) Non-aggregated Aβ42 without Aβ42 aggregates
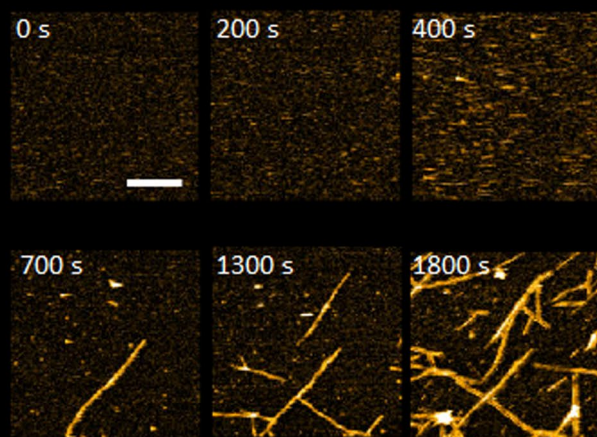
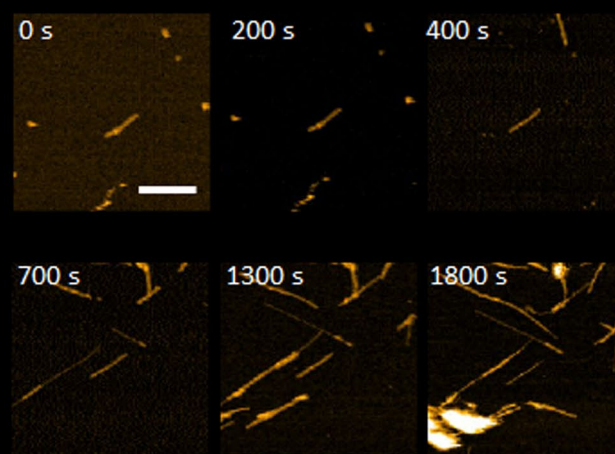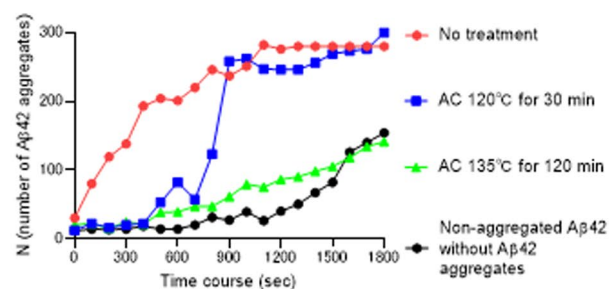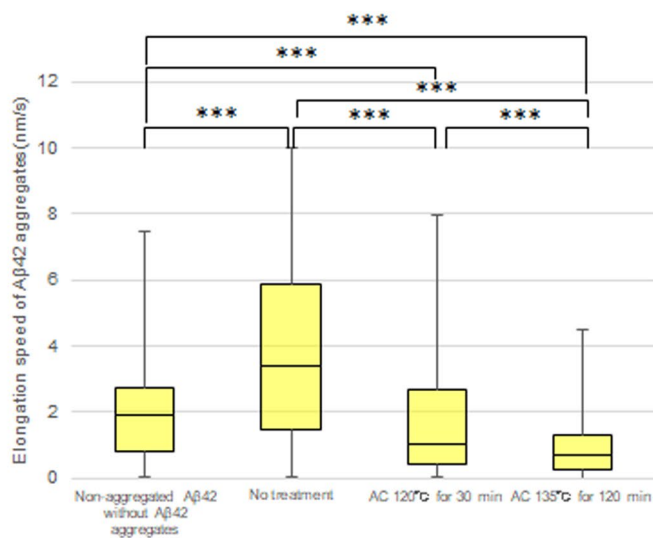(b) No treatment
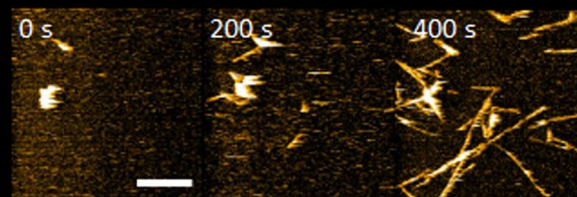
(c) AC 120℃ for 30 min
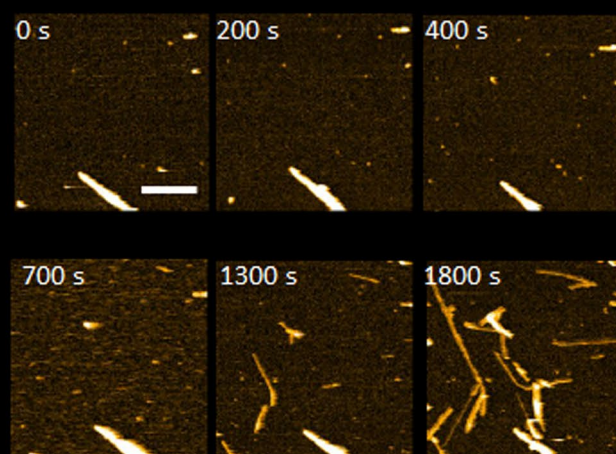
(d) AC 135℃ for 120 min

(e) The cumulative number of Aβ42 aggregates attached on mica

(f) Elongation speed of Aβ42 aggregates attached on mica

FIGURE 3 Observation of the seeding effects of amyloid beta-protein 1–42 (Aβ42) aggregates with high-speed atomic force microscopy (HS-AFM) and analysis of the cumulative number and elongation speed of Aβ42 aggregates. We show four different groups of HS-AFM images as follows: (a) Aβ42 with filtration incubated without Aβ42 aggregates (non-aggregated Aβ42 without Aβ42 aggregates); (b) Aβ42 with filtration incubated with untreated Aβ42 aggregates (no treatment); (c) Aβ42 with filtration incubated with autoclaved Aβ42 aggregates treated at 120°C for 30 min (AC 120°C for 30 min); (d) Aβ42 with filtration incubated with autoclaved Aβ42 aggregates treated at 135°C for 120 min (AC 135°C for 120 min). The HS-AFM images are partially cropped (frame rates, 0.1 frames per second; pixel sizes, 400 × 400; scale bars, 200 nm; Z scale 15 nm) (a–d). The number of Aβ42 aggregates in each four group (non-aggregated Aβ42 without Aβ42 aggregates, no treatment, AC 120°C for 30 min, and AC 135°C for 120 min) is counted every 100 s (e). The elongation speed of Aβ42 aggregates in each four group (non-aggregated Aβ42 without Aβ42 aggregates, no treatment, AC 120°C for 30 min, and AC 135°C for 120 min) is shown in the box-and-whisker plot (f). Boxes extend from the 25th to the 75th percentile values (f). The line in the box represents the median values. The whiskers are drawn from the minimum to the 25th percentile value and from the 75th percentile value to the maximum. Asterisks indicate statistical significance between the two groups indicated by brackets (*$p < 0.05$, **$p < 0.01$, ***$p < 0.001$) (n = number of Aβ42 aggregates) (Brunner–Munzel test)
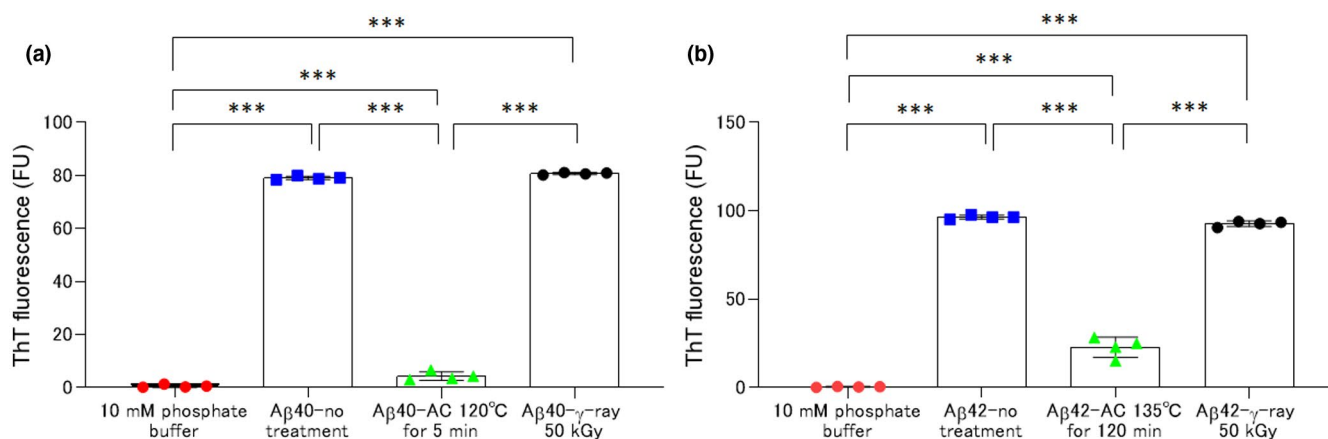

FIGURE 4 Thioflavin T (ThT) fluorescence of amyloid beta-protein (Aβ) aggregates after different treatments. We show four different samples of Aβ1-40 (Aβ40) aggregates (a) and Aβ1-42 (Aβ42) aggregates (b) as follows: (a) 10 mM phosphate buffer, untreated Aβ40 aggregates (Aβ40-no treatment), autoclaved Aβ40 aggregates treated at 120°C for 5 min (Aβ40-AC 120°C for 5 min), and Aβ40 aggregates with γ-ray irradiation at 50 kGy (Aβ40-γ-ray 50 kGy); (b), 10 mM phosphate buffer, untreated Aβ42 aggregates (Aβ42-no treatment), autoclaved Aβ42 aggregates treated at 135°C for 120 min (Aβ42-AC 135°C for 120 min), and Aβ42 aggregates with γ-ray irradiation at 50 kGy (Aβ42-γ-ray 50 kGy). Four datasets of the ThT fluorescence in each sample are plotted in bar graphs indicating mean values of the ThT fluorescence, while the error bars indicate standard deviations (a and b). Asterisks indicate statistical significance of the difference between the two groups (*$p < 0.05$, **$p < 0.01$, ***$p < 0.001$) (one-way factorial ANOVA with Tukey post hoc comparisons)

pre-determined samples size calculation was applied, and the sample sizes were based on previous studies (Ono et al., 2012; Watanabe-Nakayama et al., 2016, 2020).

3 | RESULTS

3.1 | Evaluation of Aβ seeding activity using ThT assays

The temporal changes in the ThT fluorescence of six different types of Aβ40 assemblies containing non-aggregated Aβ40 and untreated or autoclaved Aβ40 aggregates are shown in Figure 1a, b. AC conditions for Aβ40 aggregates were changed as follows: temperatures: 105, 110, 115, and 120°C; exposure times: 5, 15, 30, and 60 min. The ThT fluorescence of the Aβ40 assembly containing non-aggregated Aβ40 without Aβ40 aggregates demonstrated a sigmoidal curve,

characterized by a lag-time of 0–12 h, followed by an elongation time of 0.5–7 days (Figure 1a, b). Incubation of the Aβ40 assembly containing non-aggregated Aβ40 and Aβ40 aggregates without AC (Aβ40-no treatment) resulted in a hyperbolic increase in the ThT fluorescence, characterized by a 0–4 h period of elongation time followed by a plateau state of the maximum fluorescence intensity after 4–24 h (Figure 1a, b). The increasing speed of ThT fluorescence of the Aβ40 assemblies containing non-aggregated Aβ40 and autoclaved Aβ40 aggregates was slower at AC conditions of higher temperatures or longer exposure times (Figure 1a, b). There were significant differences in SD_{50} among non-aggregated Aβ40 without Aβ40 aggregates and Aβ40-no treatment ($p < 0.001$), and Aβ40 assemblies containing non-aggregated Aβ40 and autoclaved Aβ40 aggregates treated at 105°C for 5 min ($p < 0.001$), 110°C for 5 min ($p < 0.001$), and 105°C for 15 min ($p < 0.001$) (one-way ANOVA with Dunnett's post hoc comparisons, $f = 108.7$ and 50.7) (Figure 1i, j). In contrast, there were no significant differences in
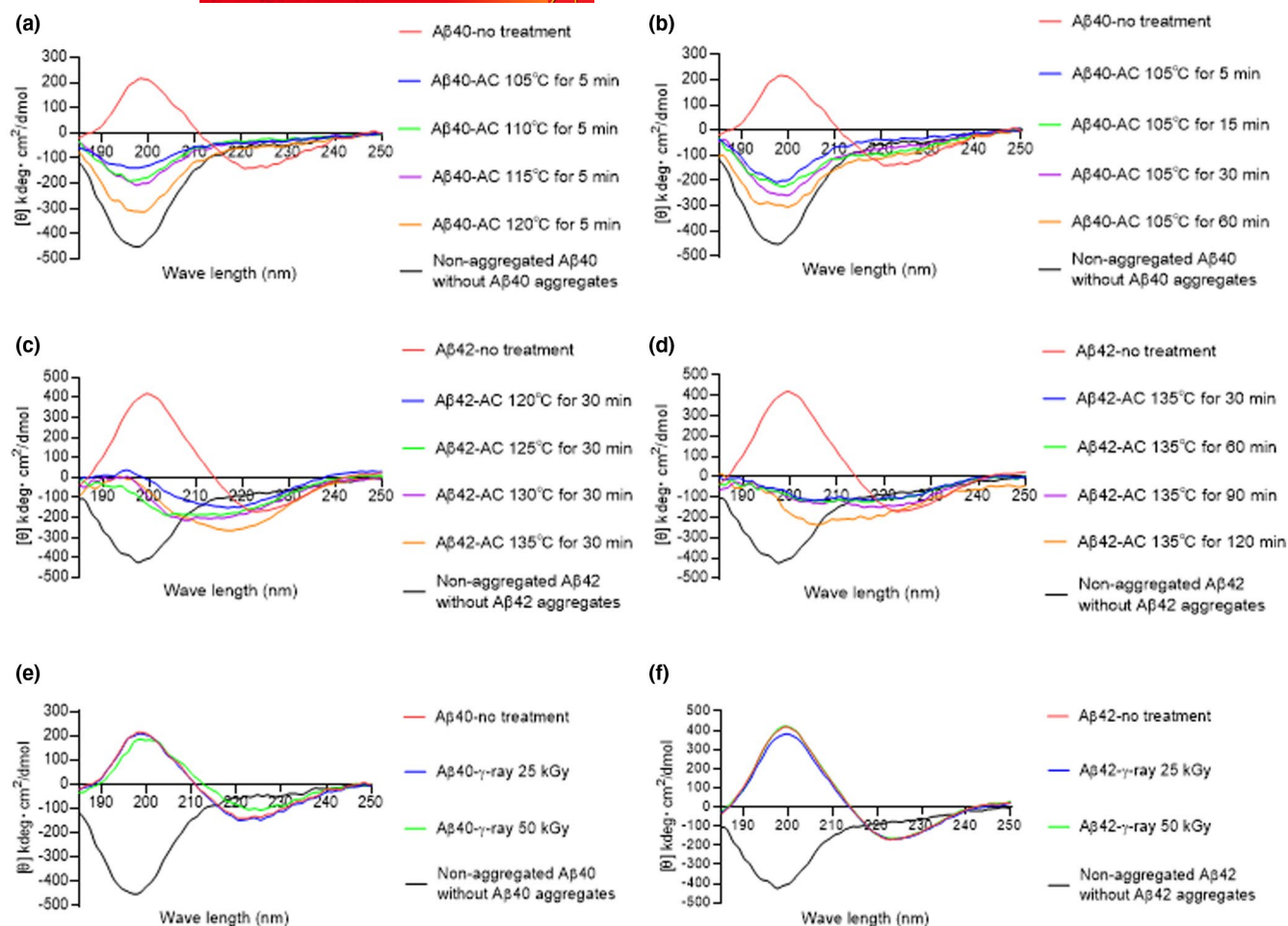
FIGURE 5 Circular dichroism (CD) spectral patterns of non-aggregated amyloid beta-protein (Aβ) and Aβ aggregates treated with autoclaving (AC) or γ-ray irradiation. We show six different types of CD spectral curves in Aβ1-40 (Aβ40) assemblies (a, b, and e) and Aβ1-42 (Aβ42) assemblies (c, d, and f) as follows: (a) 1. Aβ40 aggregates without AC (Aβ40-no treatment); 2–5. Autoclaved Aβ40 aggregates treated at 105°C for 5 min (Aβ40-AC 105°C for 5 min), 110°C for 5 min (Aβ40-AC 110°C for 5 min), 115°C for 5 min (Aβ40-AC 115°C for 5 min), and 120°C for 5 min (Aβ40-AC 120°C for 5 min); and 6. Non-aggregated Aβ40 without Aβ40 aggregates; (b), 1. Aβ40-no treatment; 2–5. Autoclaved Aβ40 aggregates treated at 105°C for 5 min (Aβ40-AC 105°C for 5 min), 105°C for 15 min (Aβ40-AC 105°C for 15 min), 105°C for 30 min (Aβ40-AC 105°C for 30 min), and 105°C for 60 min (Aβ40-AC 105°C for 60 min); and 6. Non-aggregated Aβ40 without Aβ40 aggregates; (c) 1. Aβ42 aggregates without AC (Aβ42-no treatment); 2–5. Autoclaved Aβ42 aggregates treated at 120°C for 30 min (Aβ42-AC 120°C for 30 min), 125°C for 30 min (Aβ42-AC 125°C for 30 min), 130°C for 30 min (Aβ42-AC 130°C for 30 min), and 135°C for 30 min (Aβ42-AC 135°C for 30 min); and 6. Non-aggregated Aβ42 without Aβ42 aggregates; (d) 1. Aβ42-no treatment; 2–5. Autoclaved Aβ42 aggregates treated at 135°C for 30 min (Aβ42-AC 135°C for 30 min), 135°C for 60 min (Aβ42-AC 135°C for 60 min), 135°C for 90 min (Aβ42-AC 135°C for 90 min), and 135°C for 120 min (Aβ42-AC 135°C for 120 min); and 6. Non-aggregated Aβ42 without Aβ42 aggregates; (e) 1. Aβ40-no treatment; 2, 3. Aβ40 aggregates with γ-ray irradiation at 25 kGy (Aβ40-γ-ray 25 kGy) and 50 kGy (Aβ40-γ-ray 50 kGy); and 4. Non-aggregated Aβ40 without Aβ40 aggregates; (f) 1. Aβ42-no treatment; 2, 3. Aβ42 aggregates with γ-ray irradiation at 25 kGy (Aβ42-γ-ray 25 kGy) and 50 kGy (Aβ42-γ-ray 50 kGy); and 4. Non-aggregated Aβ42 without Aβ42 aggregates. Average values of ten CD spectra measurements in each Aβ aggregate are plotted (a–f)

SD_{50} among non-aggregated Aβ40 without Aβ40 aggregates and Aβ40 assemblies containing non-aggregated Aβ40 and autoclaved Aβ40 aggregates treated at 115°C for 5 min ($p = 0.51$), 120°C for 5 min ($p = 0.15$), 105°C for 30 min ($p = 0.44$), and 105°C for 60 min ($p > 0.99$) (one-way ANOVA with Dunnett's post hoc comparisons, $f = 108.7$ and 50.7) (Figure 1i, j).

The temporal changes in the ThT fluorescence of six different types of Aβ42 assemblies containing non-aggregated Aβ42 and untreated or autoclaved Aβ42 aggregates are shown in Figure 1c, d. AC conditions for Aβ42 aggregates were same as those for Aβ40

aggregates as follows: temperatures: 105, 110, 115, and 120°C; exposure times: 5, 15, 30, and 60 min. The ThT fluorescence of the Aβ42 assembly containing non-aggregated Aβ42 without Aβ42 aggregates showed a sigmoidal curve, characterized by an elongation time of 0–4 h, followed by a plateau state of the maximum fluorescence intensity after 4–12 h (Figure 1c, d). Incubation of the Aβ42 assembly containing non-aggregated Aβ42 and Aβ42 aggregates without AC (Aβ42-no treatment) showed a hyperbolic increase in ThT fluorescence, characterized by reaching the maximum fluorescence intensity after 30 min, followed by a continuous plateau state
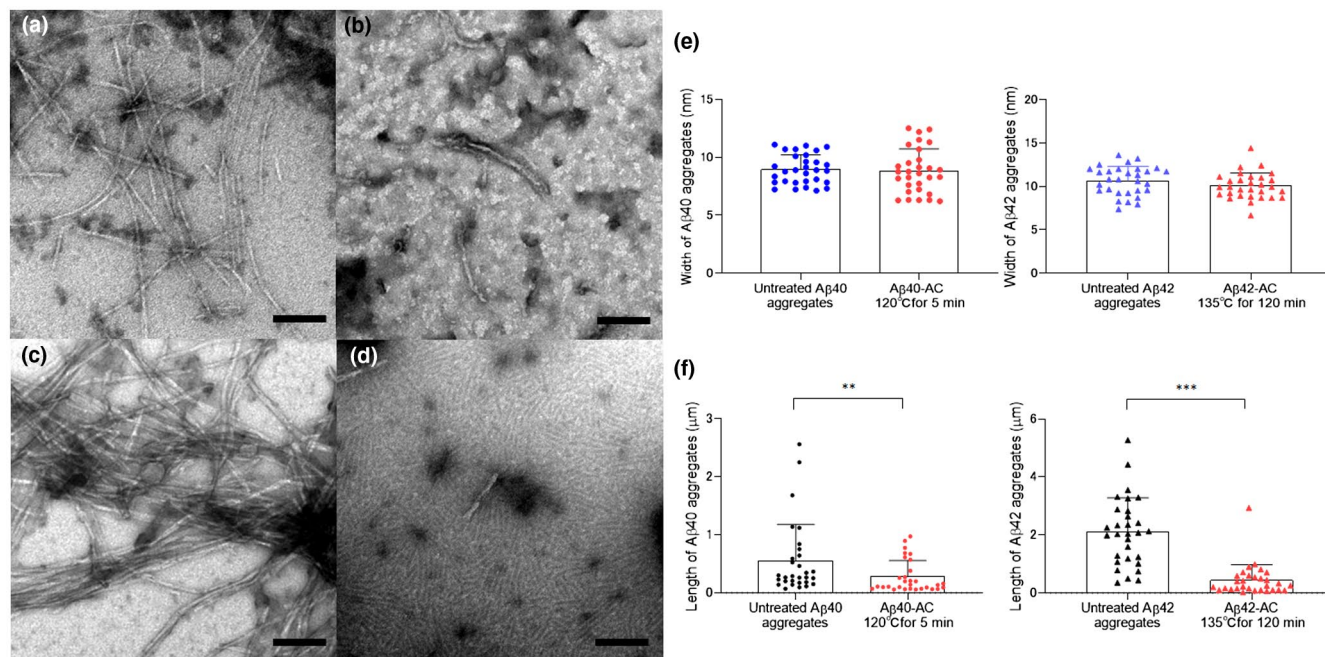
FIGURE 6 Electron microscopy (EM) images of untreated and autoclaved amyloid beta-protein (Aβ) aggregates with fibril-like structures. We show untreated and autoclaved Aβ aggregates with fibril-like structures in Aβ1-40 (Aβ40) and Aβ1-42 (Aβ42) as follows: (a) Aβ40 aggregates with fibril-like structures without autoclaving (AC) (untreated Aβ40 aggregates); (b) Autoclaved Aβ40 aggregates with fibril-like structures treated at 120°C for 5 min (Aβ40-AC 120°C for 5 min); (c) Aβ42 aggregates with fibril-like structures without AC (untreated Aβ42 aggregates); (d) Autoclaved Aβ42 aggregates with fibril-like structures treated at 135°C for 120 min (Aβ42-AC 135°C for 120 min). The magnification of EM images is 30 000× (a–d) (Scale bars, 100 nm). The results of the width and length of Aβ aggregates with fibril-like structures in EM images are shown in (e) and (f) ($n = 30$). All datasets of the width and length of Aβ aggregates with fibril-like structures are plotted in the bar graphs showing the mean values of each measurement, while the error bars indicate standard deviations. Asterisks indicate statistical significances between the two groups indicated by brackets (*$p < 0.05$, **$p < 0.01$, ***$p < 0.001$) ($n =$ number of Aβ aggregates with fibril-like structures)

after 0.5–12 h (Figure 1c, d). Incubation of non-aggregated Aβ42 with autoclaved Aβ42 aggregates also demonstrated a hyperbolic increase in the ThT fluorescence (Figure 1c, d), and there were significant differences in SD_{50} among non-aggregated Aβ42 without Aβ42 aggregates and Aβ42-no treatment, and Aβ42 assemblies containing non-aggregated Aβ42 and autoclaved Aβ42 aggregates treated at 105°C, 110°C, 115°C, and 120°C for 5 min, and 105°C for 15 min, 30 min, and 60 min (one-way ANOVA with Dunnett's post hoc comparisons, $p < 0.001$, $f = 276.2$ and 276) (Figure 1k, l).

The treatments for Aβ42 aggregates under other AC conditions were examined because the Aβ42 aggregates were not significantly inactivated after AC under the same conditions as Aβ40 aggregates (Figure 1i–l). To examine the seeding activities of the autoclaved Aβ42 aggregates treated at high temperatures or long exposure times, the temporal changes in the ThT fluorescence of six different types of Aβ42 assemblies containing non-aggregated Aβ42 and untreated or autoclaved Aβ42 aggregates are shown in Figure 1e, f. AC conditions for Aβ42 aggregates were changed as follows: temperatures: 120 125, 130, and 135°C; exposure times: 30, 60, 90, and 120 min. The increase in the ThT fluorescence of the Aβ42 assemblies containing non-aggregated Aβ42 and autoclaved Aβ42 aggregates was slower than that in the mixed samples of Aβ42-no treatment. There were significant differences in SD_{50} among non-aggregated Aβ42

without Aβ42 aggregates and Aβ42-no treatment ($p < 0.001$), and Aβ42 assemblies containing non-aggregated Aβ42 and autoclaved Aβ42 aggregates treated at 120°C for 30 min ($p < 0.001$), 125°C for 30 min ($p < 0.001$), 130°C for 30 min ($p < 0.001$), 135°C for 30 min ($p = 0.0051$), and 135°C for 60 min ($p = 0.0039$) (one-way ANOVA with Dunnett's post hoc comparisons, $f = 173.2$, and 104.4) (Figure 1m, n). There were no significant differences in SD_{50} among non-aggregated Aβ42 without Aβ42 aggregates and Aβ42 assemblies containing non-aggregated Aβ42 and autoclaved Aβ42 aggregates treated at 135°C for 90 min ($p = 0.09$), and 135°C for 120 min ($p = 0.87$) (one-way ANOVA with Dunnett's post hoc comparisons, $f = 104.4$) (Figure 1n).

The temporal changes in the ThT fluorescence of Aβ assemblies containing non-aggregated Aβ and Aβ aggregates with γ-ray irradiation (25 or 50 kGy) are shown in Figure 1g (Aβ40) and 1h (Aβ42). Incubation of the Aβ assemblies containing non-aggregated Aβ and Aβ aggregates with γ-ray irradiation (25 or 50 kGy) showed hyperbolic increases in the ThT fluorescence (Figure 1g, h), and there were significant differences in SD_{50} among non-aggregated Aβ without Aβ aggregates and Aβ assemblies containing non-aggregated Aβ and Aβ aggregates with γ-ray irradiation (25 or 50 kGy) in both Aβ40 and Aβ42 (one-way ANOVA with Dunnett's post hoc comparisons, $p < 0.001$, $f = 46.7$ and 260.4) (Figure 1o, p). The mean value of the

ThT fluorescence of the sample buffers was 20.6 ± 3.6 FU (mean value ± SD) using 5 μM ThT solutions.

Another ThT assay was performed using Aβ aggregates autoclaved at different concentrations of Aβ aggregates (Figure 2a, b). The temporal changes in the ThT fluorescence of six different types of Aβ assemblies containing non-aggregated Aβ and untreated or autoclaved Aβ aggregates are shown in Figure 2a (Aβ40) and 2b (Aβ42). Concentrations for Aβ aggregates during AC were changed as follows: 0.25, 2.5, 25, and 250 μM. The concentrations of Aβ aggregates, which were added to non-aggregated Aβ, were same in all Aβ assemblies in both Aβ40 and Aβ42. The ThT fluorescence of non-aggregated Aβ without Aβ aggregates demonstrated sigmoidal curves in both Aβ40 and Aβ42 (Figure 2a, b). Incubation of the mixed samples of Aβ40-no treatment and Aβ42-no treatment resulted in hyperbolic increases in ThT fluorescence (Figure 2a, b). The increase in ThT fluorescence of Aβ assemblies containing non-aggregated Aβ and autoclaved Aβ aggregates was slower depending on lower concentrations of Aβ aggregates after treatment with AC (Figure 2a, b). There were significant differences in SD_{50} between Aβ40-no treatment and non-aggregated Aβ40 without Aβ40 aggregates (one-way ANOVA with Tukey post hoc comparisons, $p = 0.03$, $f = 3.8$) (Figure 2c). However, there were no significant differences in SD_{50} among Aβ40-no treatment and Aβ40 assemblies containing non-aggregated Aβ40 and autoclaved Aβ40 aggregates treated at a concentration of 250 μM ($p > 0.99$), 25 μM ($p > 0.99$), 2.5 μM ($p > 0.99$), and 0.25 μM ($p = 0.54$) (one-way ANOVA with Tukey post hoc comparisons, $f = 3.8$) (Figure 2c). In Aβ42, there were significant differences in SD_{50} among Aβ42-no treatment and Aβ42 assemblies containing non-aggregated Aβ42 and autoclaved Aβ42 aggregates treated at a concentration of 0.25 μM and non-aggregated Aβ42 without Aβ42 aggregates (one-way ANOVA with Tukey post hoc comparisons, $p < 0.001$, $f = 44.4$). There was no significant differences in SD_{50} among Aβ42-no treatment and Aβ42 assemblies containing non-aggregated Aβ42 and autoclaved Aβ42 aggregates treated at a concentration of 250 μM ($p = 0.99$), 25 μM ($p = 0.57$), and 2.5 μM ($p = 0.53$) (one-way ANOVA with Tukey post hoc comparisons, $f = 44.4$) (Figure 2d). The mean value of the ThT fluorescence of the sample buffers was 43.2 ± 4.8 FU (mean value ± SD) using 10 μM ThT solutions.

3.2 | Observation of the elongation of Aβ42 aggregates using HS-AFM

Four different groups of HS-AFM images are shown in Figure 3 as follows: Aβ42 with filtration incubated without Aβ42 aggregates (non-aggregated Aβ42 without Aβ42 aggregates) (Figure 3a); Aβ42 with filtration incubated with untreated Aβ42 aggregates (no treatment) (Figure 3b);Aβ42 with filtration incubated with autoclaved Aβ42 aggregates treated at 120°C for 30 min (AC 120°C for 30 min) (Figure 3c); Aβ42 with filtration incubated with autoclaved Aβ42 aggregates treated at 135°C for 120 min (AC 135°C for 120 min)

(Figure 3d). When non-aggregated Aβ42 without Aβ42 aggregates was incubated in the sample chamber of HS-AFM, no Aβ42 aggregates was observed from 0 to 690 s (Figure 3a). A small number of Aβ42 aggregates appeared 700 s after incubation was started, and they subsequently increased in numbers with rapid elongation (Figure 3a). The images of mixed samples of no treatment showed a significant amount of Aβ42 aggregates immediately after the incubation was started (Figure 3b). A significant amount of Aβ42 aggregates in the mixed samples of no treatment showed rapid elongation (Figure 3b). On the other hand, only few Aβ42 aggregates appeared in the mixed samples of AC 120°C for 30 min and AC 135°C for 120 min (Figure 3c, d). Aβ42 aggregates in the mixed samples of AC 120°C for 30 min and AC 135°C for 120 min showed little elongation from the Aβ42 aggregates (Figure 3c, d).

The cumulative number of Aβ42 aggregates in the mixed samples of no treatment increased and reached the maximum number of Aβ aggregates at 1100 s, followed by a plateau state until 1800 s ($n = 280$, n: the number of Aβ42 aggregates) (Figure 3e). The cumulative number of Aβ42 aggregates in the mixed samples at AC 120°C for 30 min demonstrated a sigmoidal curve, characterized by a lag-time (0–400 s) followed by an elongation time (400–1000 s). The sigmoidal curve reached a plateau with the maximum number of Aβ aggregates obtained after 1000 s ($n = 300$) (Figure 3e). The cumulative number of Aβ42 aggregates in the mixed samples of AC 135°C for 120 min and non-aggregated Aβ42 without Aβ42 aggregates gradually increased (Figure 3e). The numbers of Aβ aggregates at 1800 s in the mixed samples of AC 135°C for 120 min and non-aggregated Aβ42 without Aβ42 aggregates were 141 (AC 135°C for 120 min) and 154 (non-aggregated Aβ42 without Aβ42 aggregates) (Figure 3e). The elongation speed of Aβ42 aggregates in the mixed samples of no treatment was significantly faster than that in the mixed samples of AC 120°C for 30 min, 135°C for 120 min, and non-aggregated Aβ42 without Aβ42 aggregates (Brunner–Munzel tests, $p < 0.001$, $df > 402.7$) (Figure 3f). The elongation speed of Aβ42 aggregates in the mixed samples of AC 120°C for 30 min was significantly faster than that in the mixed samples of AC 135°C for 120 min (Brunner–Munzel tests, $p < 0.001$, $df = 350.9$) (Figure 3f). The elongation speed of Aβ42 aggregates in the mixed samples of AC 120°C for 30 min and AC 135°C for 120 min was significantly slower than that in the mixed samples of non-aggregated Aβ42 without Aβ42 aggregates (Brunner–Munzel tests, $p < 0.001$, $df > 283.8$) (Figure 3f).

3.3 | ThT fluorescence of Aβ aggregates after treatment with AC or γ-ray irradiation

The ThT fluorescence of four different samples is shown in Figure 4a (Aβ40) and 4b (Aβ42) as follows: Figure 4a, 10 mM phosphate buffer, untreated Aβ40 aggregates (Aβ40-no treatment), autoclaved Aβ40 aggregates treated at 120°C for 5 min (Aβ40-AC 120°C for 5 min), and Aβ40 aggregates with γ-ray irradiation at 50 kGy (Aβ40-γ-ray 50 kGy); Figure 4b, 10 mM phosphate buffer, untreated Aβ42

aggregates (Aβ42-no treatment), autoclaved Aβ42 aggregates treated at 135°C for 120 min (Aβ42-AC 135°C for 120 min), and Aβ42 aggregates with γ-ray irradiation at 50 kGy (Aβ42-γ-ray 50 kGy). The ThT fluorescence of 10 mM phosphate buffer showed only a slight increase (Figure 4a), whereas those of the mixed samples of Aβ40-no treatment, Aβ40-AC 120°C for 5 min and Aβ40-γ-ray 50 kGy showed significant increases compared to that of the 10 mM phosphate buffer (one-way ANOVA with Tukey post hoc comparisons, $p < 0.001$, $f = 9668$) (Figure 4a). The ThT fluorescence of the mixed samples of Aβ40-AC at 120°C for 5 min was significantly reduced compared to that of the mixed samples of Aβ40-no treatment and Aβ40-γ-ray 50 kGy (one-way ANOVA with Tukey post hoc comparisons, $p < 0.001$, $f = 9668$) (Figure 4a). There was no significant difference in ThT fluorescence between Aβ40-no treatment and Aβ40-γ-ray at 50 kGy (one-way ANOVA with Tukey post hoc comparisons, $p = 0.11$, $f = 9668$) (Figure 4a). Similar results were obtained for the Aβ42 aggregates (Figure 4b). The mean value of the ThT fluorescence of the sample buffers was 21.0 ± 2.3 FU (mean value ± SD) using 5 μM ThT solutions.

3.4 | Spectral patterns of Aβ aggregates in CD spectroscopy

Both non-aggregated Aβ40 and non-aggregated Aβ42 displayed spectral patterns consistent with those of random coil structures (Figure 5a–f). In contrast, both untreated Aβ40 aggregates and untreated Aβ42 aggregates demonstrated spectral patterns consistent with those of β-sheet-rich structures (Figure 5a–f). Spectral patterns of autoclaved Aβ40 aggregates indicated an increase in random coil structures with a reduction in β-sheet-rich structures (Figure 5a, b). Higher temperatures or longer exposure times of AC resulted in a higher ratio of random coil structures in autoclaved Aβ40 aggregates (Figure 5a, b). Autoclaved Aβ42 aggregates showed spectral patterns with small and convex-shaped spectral curves centered at 190–200 nm, and small and concave-shaped spectral curves centered at 200–220 nm. These spectral patterns indicate an increase in random coil structures with a reduction in β-sheet-rich structures in autoclaved Aβ42 aggregates (Figure c, d). The reduction in the amplitude of the convex-shaped spectral curves of autoclaved Aβ42 aggregates depended on higher temperatures and longer exposure times of AC. The increase in the amplitude of the concave-shaped spectral curves of autoclaved Aβ42 aggregates also depended on higher temperatures and longer exposure times of AC (Figure 5c, d). Spectral patterns of Aβ aggregates with γ-ray irradiation were similar to those of untreated Aβ aggregates in both Aβ40 and Aβ42 (Figure 5e, f).

3.5 | EM images of Aβ aggregates with fibril-like structures

Untreated Aβ aggregates with fibril-like structures demonstrated non-branched structures, and the width of untreated

Aβ aggregates with fibril-like structures (mean value ± SD) was 8.9 ± 1.3 nm ($n = 30$, n: the number of Aβ aggregates with fibril-like structures) (Aβ40) and 10.6 ± 1.6 nm ($n = 30$) (Aβ42) (Figure 6a, c, and e), which were similar to that of Aβ aggregates with fibril-like structures seen in previous reports (Ono et al., 2003, 2012). Autoclaved Aβ aggregates with fibril-like structures also showed non-branched structures, and the width of autoclaved Aβ aggregates with fibril-like structures (mean value ± SD) was 8.8 ± 1.9 nm ($n = 30$) (Aβ40) and 10.0 ± 1.5 nm ($n = 30$) (Aβ42) (Figure 6b, d, and e). There were no significant differences in the width of Aβ aggregates with fibril-like structures between untreated and autoclaved Aβ aggregates in either Aβ40 ($p = 0.75$, $t = 0.32$, $df = 58$) and Aβ42 ($p = 0.14$, $t = 1.5$, $df = 58$) (t-test) (Figure 6e). The length of untreated Aβ aggregates with fibril-like structures (mean value ± SD) was 0.55 ± 0.62 μm ($n = 30$) (Aβ40) and 2.1 ± 1.2 μm ($n = 30$) (Aβ42) (Figure 6f), and the length of autoclaved Aβ aggregates with fibril-like structures (mean value ± SD) was 0.28 ± 0.28 μm ($n = 30$) (Aβ40) and 0.43 ± 0.55 μm ($n = 30$) (Aβ42) (Figure 6f). Significant differences in the length of Aβ aggregates with fibril-like structures between untreated and autoclaved Aβ aggregates were seen in both Aβ40 ($p = 0.004$) and Aβ42 ($p < 0.001$) (Mann-Whitney U test) (Figure 6f).

4 | DISCUSSION

In this study, the seeding studies using ThT assays and HS-AFM revealed that the seeding effects of Aβ aggregates were inactivated with AC but not with γ-ray irradiation. In addition, the seeding activities of Aβ aggregates decreased with higher temperatures, longer exposure times, and lower concentrations of Aβ aggregates during treatment with AC. According to the ThT assay results, the AC conditions for inactivating both Aβ40 and Aβ42 aggregates require a temperature of 135°C or higher and an exposure time of 90 min or longer. Based on the HS-AFM observations, the rapid increase of the cumulative number of Aβ42 aggregates in the mixed samples of AC 120°C for 30 min after the lag-time may indicate that AC at 120°C for 30 min could not inhibit secondary nucleation of Aβ42 aggregates (Cohen et al., 2013; Linse, 2019; Scheidt et al., 2019; Törnquist et al., 2018). The low concentrations of Aβ42 after the polymerization of the Aβ42 aggregates in the mixed samples of non-aggregated Aβ42 without Aβ42 aggregates may be a cause of its slower elongation compared to that of Aβ42 aggregates in the mixed samples of no treatment. Regarding structural changes in post-treatment Aβ aggregates, ThT assays, CD spectroscopy, and EM imaging indicated that AC in conditions of higher temperatures and longer exposure times caused significantly reduced β-sheet-rich structures in Aβ aggregates, and longer Aβ aggregates.

The deposition of misfolded proteins in the brain is a common feature of many neurodegenerative diseases that play important roles in their pathogenesis (Kushwah et al., 2020; Thomzig et al., 2014). Accumulation of Aβ pathology in the brain is the main pathological feature of AD (Tiwari et al., 2019; Watts et al., 2018). The

molecular mechanisms of Aβ aggregation have been explained by nucleation-dependent polymerization models, which are characterized by an initial slow nucleation (a lag-time) followed by elongation time (Friesen et al., 2019). Previous studies reported that incubation of non-aggregated Aβ and untreated Aβ aggregates developed hyperbolic Aβ aggregations, which were described as an acceleration of the polymerization process with short lag-time in the seeding assays (Harper et al., 1997; Jarrett et al., 1992, 1993; Ono et al., 2012). The ThT assays and HS-AFM results indicate that AC could inactivate the seeding activities of Aβ aggregates, suggesting that the transmission of Aβ pathology among individuals could be prevented by AC.

The EM images in this study showed that the length of autoclaved Aβ aggregates with fibril-like structures was shorter than that of the untreated ones. The results indicate that AC induces fragmentation of Aβ aggregates. Fragmentation of Aβ aggregates using ultrasonic disruptors and stirring bars has been reported to increase the seeding activity of Aβ aggregates in vitro and in vivo (Falsig et al., 2008; Friesen et al., 2019; Jarrett et al., 1993; Knowles et al., 2009; Xue et al., 2009). A previous report showed that Aβ aggregates fragmented with an ultrasonicator demonstrated an increase in β-sheet structures that interacted with other Aβ aggregates (Harris., 2012). In contrast, the fragmented Aβ aggregates after AC showed a reduction in the β-sheet-rich structures and seeding activity of Aβ aggregates. Based on these results, we speculate that decreasing β-sheet-rich structures could inactivate the seeding activity of Aβ aggregates.

AC of chemical substances, including proteins, disturbs hydrogen bonding and non-polar hydrophobic interactions in chemical compounds, which are responsible for secondary and tertiary structures (David et al., 2013). Increasing the vulnerability of the steric structures through heat denaturation would lead to conformational changes, causing original function loss of the chemical substance (David et al., 2013; Donald et al., 2016). Heat denaturation occurs during AC of Aβ aggregates that led to conformational changes, particularly the reduction of β-sheet-rich structures in Aβ aggregates. Therefore, structural changes in Aβ aggregates would lead to inactivation of their seeding activity in this study. In contrast, γ-ray irradiation did not alter Aβ seeding activity in ThT assays. A previous study reported that the main molecular mechanisms of sterilization using γ-ray irradiation were cell death induced by severe DNA damage in cell nuclei (Zhang et al., 2012), indicating the inability of γ-ray irradiation to change the seeding activity of Aβ aggregates because of their lack of nucleic acids.

In this study, the seeding activity of the Aβ40 aggregates was more easily inactivated than that of Aβ42 aggregates when Aβ40 and Aβ42 aggregates were treated under the same AC conditions (temperatures: 105, 110, 115, and 120°C, exposure times: 5, 15, 30, and 60 min) (Figure 1a–d, i–l). The higher temperatures and longer exposure times under AC were required to inactivate the seeding activity of Aβ42 aggregates (Figure 1e, f, m and n). These results indicate that there are different features in the seeding activity between Aβ40 and Aβ42 aggregates. It is known that Aβ42 is highly neurotoxic and aggregates more easily than Aβ40, and Aβ42 aggregates

show higher seeding activity than Aβ40 aggregates (Chen et al., 2017; Fawzi et al., 2011; Morimoto et al., 2004; Ono et al., 2012; Srivastava et al., 2019; Tiwari et al., 2019; Zhang et al., 2012). These findings could be related to the AC conditions needed to inactivate the seeding effect of Aβ42 aggregates in the present study. Although the precise mechanisms underlying the higher seeding activity of Aβ42 aggregates compared to that of Aβ40 aggregates have yet to be elucidated, the AC-resistant characteristics of Aβ42 aggregates are speculated to be important in understanding the molecular mechanisms of Aβ aggregation.

Previous studies have demonstrated that Aβ aggregation is influenced by other compounds or different reaction buffer conditions (Korshavn et al., 2017; Schützmann et al., 2021; Sciacca et al., 2020). Dilauroyl phosphatidylcholine, a chemical used for cell membrane models, generates protofibrils and oligomers that lead to cytotoxicity (Korshavn et al., 2017; Sciacca et al., 2020). The interaction between Aβ oligomers and ganglioside-containing cell membranes accelerated the formation of neurotoxic Aβ aggregates (Kotler et al., 2014). Cross-seeding reactions between Aβ aggregates and other proteins developed heterogeneous aggregates with unique β-sheet-rich structures compared to those produced in homogenous cross-seeding reactions (Ivanova et al., 2021). Moreover, the presence of metal ions in the reaction buffers accelerates Aβ aggregation (DeToma et al., 2012). Different pH levels in the reaction buffers alter the polymerization of Aβ aggregates (Schützmann et al., 2021). Based on these reports, we speculate that AC conditions for inactivating Aβ seeding activity would change in the presence of different reaction buffer components or conditions.

Several reports have shown that misfolded proteins deposited in the brains of patients with neurodegenerative diseases, including Aβ in patients with AD, α-synuclein in PD and DLB, and PrP in prion diseases, have the potential to propagate among individuals under animal experiments (Burwinkel et al., 2018; Hamaguchi et al., 2012; Jucker et al., 2018; Langer et al., 2011; Meyer-Luehmann et al., 2006; Watts et al., 2011). Inactivation methods for PrP, such as sodium hypochlorite, NaOH, alkaline detergent, phenol, SDS, guanidine hydrochloride, trichloroacetic acid, formic acid, and hydrogen peroxide gas plasma, have been established using animal experiments (Murphy et al., 2009; Sakudo., 2020). Previous reports have also demonstrated that AC is effective in inactivating PrP (Fichet et al., 2004, 2007). A World Health Organization report (1999) on infection control guidelines for prion diseases recommend AC combined with chemical detergent for decontaminating PrP on medical devices (World Health Organization Report., 1999). In addition, a recent study reported that the seeding activity of α-synuclein was also inactivated by AC in animal experiments (Tarutani et al., 2018). However, no report exists in the examination of AC conditions for the inactivation of Aβ aggregates in vitro or in vivo.

Several decontamination methods for preventing the propagation of Aβ pathophysiologies, such as formic acid sterilization, formaldehyde fixation, boiling, and hydrogen peroxide gas plasma sterilization, have been previously examined (Eisele et al., 2009; Fritschi et al., 2014; Meyer-Luehmann et al., 2006). Boiling and

formaldehyde fixation have been reported to have no potential in the inactivation of the seeding effect of Aβ aggregates, and the inactivation treatments for brain extracts from APP23 transgenic mice with 70% formic acid for 1 h or hydrogen peroxide gas plasma sterilization using a STERRAD 100 S developed complete blocks of Aβ deposition in the brain (Eisele et al., 2009; Meyer-Luehmann et al., 2006). The precise mechanisms of hydrogen peroxide gas plasma and formic acid for inactivating Aβ pathology have not been elucidated. However, several reports demonstrated that these methods caused structural changes in the proteins, showing an increase in α-helices with a decrease in β-turn structures (Christensen et al., 2020; Sakudo et al., 2013). Gas plasma and formic acid sterilization have also been reported to destabilize hydrogen bonds and hydrophobic residue interactions (Christensen et al., 2020; Sakudo et al., 2013). A study using a fourier transform infrared spectrometer demonstrated that heating between 35 and 85°C did not result in secondary structural changes (Sakudo et al., 2013). These reports indicate that conformational changes in Aβ aggregates are related to seeding activity inactivation, and these findings are similar to the structural changes observed in autoclaved Aβ aggregates in the present study. AC would develop structural changes in PrP and α-synuclein aggregates, thereby inactivating their seeding activities. However, no studies have examined the structural and functional features of PrP and α-synuclein after AC in vitro. Structural changes would be related to reduce the seeding activity of misfolded proteins.

There are several limitations in this study. First, the Aβ aggregation process was not examined in biological situations using cultured cells and animal models. Moreover, continuous observations of the elongation of Aβ42 aggregates using HS-AFM were monitored on silicon-containing mica, which does not exist in biological systems. To establish effective methods in preventing the propagation of Aβ pathology among individuals, it is important to confirm the interaction of Aβ aggregates with biological materials. Second, in vitro experiments were performed under a single reaction buffer condition. The ThT assays, CD spectroscopy, and EM experiments used mixed buffers containing Aβ aggregates and 10 mM phosphate buffer with a pH level of 7.4. The elongation of Aβ42 aggregates using HS-AFM was monitored in mixed buffers containing 10 mM phosphate buffer and 100 mM NaCl. This contributes to relatively restrictive results, and there is speculation that different conditions of the reaction buffers containing Aβ aggregates would show different AC conditions to inactivate the seeding activities of Aβ aggregates. Third, the seeding activities and structural features of Aβ aggregates were evaluated without other amyloid protein species. Previous reports demonstrated that amyloid proteins, including Aβ, α-synuclein, and PrP, showed similar conformational changes to β-sheet-rich structures in the polymerization process and pathological propagation among individuals. Although amyloid proteins have similar mechanisms in reducing seeding activities, the properties of each amyloid protein may have different features among amyloid proteins. Fourth, biomolecular investigations using nuclear magnetic resonance and cryo-electron micrography were not performed in this study.

In conclusion, AC decreases β-sheet-rich structures in Aβ aggregates, thereby inactivating the Aβ seeding activity. Treatment with AC at 135°C for 90 min was required for the inactivation of Aβ40 and Aβ42 seeding activities in the present in vitro study. Conformational changes that reduce β-sheet-rich structures are important in understanding the underlying molecular mechanisms that inactivate the seeding activity of Aβ aggregates. Future studies may focus on the role of AC procedures in preventing the propagation of pathogenic Aβ aggregates among individuals. The effects of AC on the inactivation of Aβ seeding activities also need to be further clarified with research.

CONFLICT OF INTEREST

The authors declare no conflicts of interest in this research.

AUTHOR CONTRIBUTIONS

Conceptualization: H.N., T.H., and M.Y. Methodology: H.N., T.I., and T.W. Resources: T.W. Investigation: H.N., T.I., and T.W. Data curation: H.N. Formal Analysis: H.N. Writing - Original Draft: H.N. Writing - Review & Editing: T.H., T.I., T.W., K.O., and M.Y. Visualization: H.N., T.H., T.I., T.W., K.O., and M.Y. Supervision: M.Y. Project Administration: M.Y. Funding Acquisition: T.H., and M.Y.

OPEN RESEARCH BADGES

This article has earned an Open Materials and an Open Data badge because it provided all relevant information to reproduce the study in the manuscript, and for making publicly available the digitally-shareable data necessary to reproduce the reported results. The data that support the findings of this study are openly available in OSF site at osf.io/g4m7q.

ORCID

Hiroto Nakano https://orcid.org/0000-0002-3958-7019
Tsuyoshi Hamaguchi https://orcid.org/0000-0002-1126-3776
Tokuhei Ikeda https://orcid.org/0000-0002-5135-0444
Takahiro Watanabe-Nakayama https://orcid.org/0000-0001-9758-3975
Kenjiro Ono https://orcid.org/0000-0001-8454-6155
Masahito Yamada https://orcid.org/0000-0003-2416-5662

514 | **WILEY** Journal of Neurochemistry | JNC The Official Journal of the International Society for Neurochemistry

NAKANO ET AL.

REFERENCES

Ando, T., Kodera, N., Takai, E., Maruyama, D., Saito, K., & Toda, A. (2001). A high-speed atomic force microscope for studying biological macromolecules. *Proceedings of the National Academy of Sciences of the United States of America*, 98, 12468–12472.

Banerjee, G., Adams, M. E., Jaunmuktane, Z., Alistair, L. G., Turner, B., Wani, M., Sawhney, I. M. S., Houlden, H., Mead, S., Brandner, S., & Werring, D. J. (2019). Early onset cerebral amyloid angiopathy following childhood exposure to cadaveric dura. *Annals of Neurology*, 85, 284–290.

Biancalana, M., & Koide, S. (2010). Molecular mechanism of Thioflavin-T binding to amyloid fibrils. *Biochimica Et Biophysica Acta*, 1804, 1405–1412.

Burwinkel, M., Lutzenberger, M., Heppner, F. L., Schulz-Schaeffer, W., & Baier, M. (2018). Intravenous injection of beta-amyloid seeds promotes cerebral amyloid angiopathy (CAA). *Acta Neuropathologica Communications*, 6, 23.

Cali, I., Cohen, M. L., Haïk, S., Parchi, P., Giaccone, G., Collins, S. J., Kofskey, D., Wang, H., McLean, C. A., Brandel, J. P., Privat, N., Sazdovitch, V., Duyckaerts, C., Kitamoto, T., Belay, E. D., Maddox, R. A., Tagliavini, F., Pocchiari, M., Leschek, E., ... Gambetti, P. (2018). Iatrogenic Creutzfeldt-Jakob disease with Amyloid-β pathology: An international study. *Acta Neuropathologica Communications*, 6, 5.

Cawood, E. E., Karamanos, T. K., Wilson, A. J., & Radford, S. E. (2021). Visualizing and trapping transient oligomers in amyloid assembly pathways. *Biophysical Chemistry*, 268, 106505.

Chatani, E., & Yamamoto, N. (2018). Recent progress on understanding the mechanisms of amyloid nucleation. *Biophysical Reviews*, 10, 527–534.

Chen, G. F., Xu, T. H., Yan, Y., Zhou, Y. R., Jiang, Y., Melcher, K., & Xu, H. E. (2017). Amyloid beta: Structure, biology and structure-based therapeutic development. *Acta Pharmacologica Sinica*, 38, 1205–1235.

Cheng, S. Y., Cao, Y., Rouzbehani, M., & Cheng, K. H. (2020). Coarse-grained MD simulations reveal beta-amyloid fibrils of various sizes bind to interfacial liquid-ordered and liquid-disordered regions in phase separated lipid rafts with diverse membrane-bound conformational states. *Biophysical Chemistry*, 260, 106355.

Christensen, L. F. B., Nowak, J. S., Sønderby, T. V., Frank, S. A., & Otzen, D. E. (2020). Quantitating denaturation by formic acid: Imperfect repeats are essential to the stability of the functional amyloid protein FapC. *Journal of Biological Chemistry*, 295, 13031–13046.

Cohen, S. I. A., Linse, S., Luheshi, L. M., Hellstrand, E., White, D. A., Rajah, L., Otzen, D. E., Vendruscolo, M., Dobson, C. M., & Knowles, T. P. J. (2013). Proliferation of amyloid-β42 aggregates occurs through a secondary nucleation mechanism. *Proceedings of the National Academy of Sciences of the United States of America*, 110, 9758–9763.

David, L. N., & Michael, M. C. (2013). *Lehninger principles of biochemistry* (p. 143). W. H. Freeman and Company.

DeToma, A. S., Salamekh, S., Ramamoorthy, A., & Lim, M. H. (2012). Misfolded proteins in Alzheimer's disease and type II diabetes. *Chemical Society Reviews*, 41, 608–621.

Donald, V., Judith, G. V., & Charlotte, W. P. (2016). *Fundamentals of biochemistry: life at the molecular level* (pp. 162–163). John Wiley & Sons.

Duyckaerts, C., Sazdovitch, V., Ando, K., Seilhean, D., Privat, N., Yilmaz, Z., Peckeu, L., Amar, E., Comoy, E., Maceski, A., Lehmann, S., Brion, J. P., Brandel, J. P., & Haïk, S. (2018). Neuropathology of iatrogenic Creutzfeldt-Jakob disease and immunoassay of French cadaver-sourced growth hormone batches suggest possible transmission of tauopathy and long incubation periods for the transmission of Abeta pathology. *Acta Neuropathologica*, 135, 201–212.

Ehling, R., Helbok, R., Beer, R., Lackner, P., Broessner, G., Pfausler, B., Röcken, C., Aguzzi, A., Chemelli, A., & Schmutzhard, E. (2012). Recurrent intracerebral haemorrhage after coitus: A case report of sporadic cerebral amyloid angiopathy in a younger patient. *European Journal of Neurology*, 19, e29–31.

Eisele, Y. S., Bolmont, T., Heikenwalder, M., Langer, F., Jacobson, L. H., Yan, Z. X., Roth, K., Aguzzi, A., Staufenbiel, M., Walker, L. C., & Jucker, M. (2009). Induction of cerebral beta-amyloidosis: Intracerebral versus systemic Abeta inoculation. *Proceedings of the National Academy of Sciences of the United States of America*, 106, 12926–12931.

Falsig, J., Nilsson, K. P., Knowles, T. P. J., & Aguzzi, A. (2008). Chemical and biophysical insights into the propagation of prion strains. *HFSP Journal*, 2, 332–341.

Fawzi, N. L., Ying, J., Ghirlando, R., Torchia, D. A., & Clore, G. M. (2011). Atomic-resolution dynamics on the surface of amyloid-β protofibrils probed by solution NMR. *Nature*, 480, 268–272.

Fichet, G., Comoy, E., Dehen, C., Challier, L., Antloga, K., Deslys, J. P., & McDonnell, G. (2007). Investigations of a prion infectivity assay to evaluate methods of decontamination. *Journal of Microbiol Methods*, 70, 511–518.

Fichet, G., Comoy, E., Duval, C., Antloga, K., Dehen, C., Charbonnier, A., McDonnell, G., Brown, P., Lasmézas, C. I., & Deslys, J. P. (2004). Novel methods for disinfection of prion-contaminated medical devices. *Lancet*, 364, 521–526.

Friesen, M., & Meyer-Luehmann, M. (2019). Aβ seeding as a tool to study cerebral amyloidosis and associated pathology. *Frontiers in Molecular Neuroscience*, 12, 233.

Fritschi, S. K., Cintron, A., Ye, L., Mahler, J., Bühler, A., Baumann, F., Neumann, M., Nilsson, K. P. R., Hammarström, P., Walker, L. C., & Jucker, M. (2014). Aβ seeds resist inactivation by formaldehyde. *Acta Neuropathologica*, 128, 477–484.

Frontzek, K., Lutz, M. I., Aguzzi, A., Kovacs, G. G., & Budka, H. (2016). Amyloid-β pathology and cerebral amyloid angiopathy are frequent in iatrogenic Creutzfeldt-Jakob disease after dural grafting. *Swiss Medical Weekly*, 146, w14287.

Hamaguchi, T., Eisele, Y. S., Varvel, N. H., Lamb, B. T., Walker, L. C., & Jucker, M. (2012). The presence of Aβ seeds, and not age per se, is critical to the initiation of Aβ deposition in the brain. *Acta Neuropathologica*, 123, 31–37.

Hamaguchi, T., Komatsu, J., Sakai, K., Noguchi-Shinohara, M., Aoki, S., Ikeuchi, T., & Yamada, M. (2019). Cerebral hemorrhagic stroke associated with cerebral amyloid angiopathy in young adults about 3 decades after neurosurgeries in their infancy. *Journal of the Neurological Sciences*, 399, 3–5.

Hamaguchi, T., Taniguchi, Y., Sakai, K., Kitamoto, T., Takao, M., Murayama, S., Iwasaki, Y., Yoshida, M., Shimizu, H., Kakita, A., Takahashi, H., Suzuki, H., Naiki, H., Sanjo, N., Mizusawa, H., & Yamada, M. (2016). Significant association of cadaveric dura mater grafting with subpial Aβ deposition and meningeal amyloid angiopathy. *Acta Neuropathologica*, 132, 313–315.

Harper, J. D., & Lansbury, P. T. Jr. (1997). Models of amyloid seeding in Alzheimer's disease and scrapie: Mechanistic truths and physiological consequences of the time-dependent solubility of amyloid proteins. *Annual Review of Biochemistry*, 66, 385–407.

Harrell, C. R., Djonov, V., Fellabaum, C., & Volarevic, V. (2018). Risks of using sterilization by gamma radiation: the other side of the coin. *Internation Journal of Medical Sciences*, 15, 274–279.

Harris, J. R. (2012). *Protein aggregation and fibrillogenesis in cerebral and systemic amyloid disease* (p. 37). Springer.

Hervé, D., Porché, M., Cabrejo, L., Guidoux, C., Tournier-Lasserve, E., Nicolas, G., Adle-Biassette, H., Plu, I., Chabriat, H., & Duyckaerts, C. (2018). Fatal Aβ cerebral amyloid angiopathy 4 decades after a dural graft at the age of 2 years. *Acta Neuropathologica*, 135, 801–803.

Hoshino, M. (2017). Fibril formation from the amyloid-β peptide is governed by a dynamic equilibrium involving association and dissociation of the monomer. *Biophysical Reviews*, 9, 9–16.

Ivanova, M. I., Lin, Y., Lee, Y. H., Zheng, J., & Ramamoorthy, A. (2021). Biophysical processes underlying cross-seeding in amyloid

aggregation and implications in amyloid pathology. *Biophysical Chemistry*, 269, 106507.

Jarrett, J. T., & Lansbury, L. P. T. Jr. (1992). Amyloid fibril formation requires a chemically discriminating nucleation event: Studies of an amyloidogenic sequence from the bacterial protein OsmB. *Biochemistry*, 31, 12345–12352.

Jarrett, J. T., & Lansbury, L. P. T. Jr. (1993). Seeding "one-dimensional crystallization" of amyloid: A pathogenic mechanism in Alzheimer's disease and scrapie? *Cell*, 73, 1055–1058.

Jaunmuktane, Z., Mead, S., Ellis, M., Wadsworth, J. D. F., Nicoll, A. J., Kenny, J., Launchbury, F., Linehan, J., Richard-Loendt, A., Walker, A. S., Rudge, P., Collinge, J., & Brandner, S. (2015). Evidence for human transmission of amyloid-β pathology and cerebral amyloid angiopathy. *Nature*, 525, 247–250.

Jaunmuktane, Z., Quaegebeur, A., Taipa, R., Viana-Baptista, M., Barbosa, R., Koriath, C., Sciot, R., Mead, S., & Brandner, S. (2018). Evidence of amyloid-β cerebral amyloid angiopathy transmission through neurosurgery. *Acta Neuropathologica*, 135, 671–679.

Jucker, M., & Walker, L. C. (2018). Propagation and spread of pathogenic protein assemblies in neurodegenerative diseases. *Nature Neuroscience*, 21, 1341–1349.

Knowles, T. P. J., Waudby, C. A., Devlin, G. L., Cohen, S. I. A., Aguzzi, A., Vendruscolo, M., Terentjev, E. M., Welland, M. E., & Dobson, C. M. (2009). An analytical solution to the kinetics of breakable filament assembly. *Science*, 326, 1533–1537.

Korshavn, K. J., Satriano, C., Lin, Y., Zhang, R., Dulchavsky, M., Bhunia, A., Ivanova, M. I., Lee, Y. H., La Rosa, C., Lim, M. H., & Ramamoorthy, A. (2017). Reduced lipid bilayer thickness regulates the aggregation and cytotoxicity of amyloid-β. *Journal of Biological Chemistry*, 292, 4638–4650.

Kotler, S. A., Walsh, P., Brender, J. R., & Ramamoorthy, A. (2014). Differences between amyloid-β aggregation in solution and on the membrane: Insights into elucidation of the mechanistic details of Alzheimer's disease. *Chemical Society Reviews*, 43, 6692–6700.

Kovacs, G. G., Lutz, M. I., Ricken, G., Ströbel, T., Höftberger, R., Preusser, M., Regelsberger, G., Hönigschnabl, S., Reiner, A., Fischer, P., Budka, H., & Hainfellner, J. A. (2016). Dura mater is a potential source of Aβ seeds. *Acta Neuropathologica*, 131, 911–923.

Kushwah, N., Jain, V., & Yadav, D. (2020). Osmolytes: A possible therapeutic molecule for ameliorating the neurodegeneration caused by protein misfolding and aggregation. *Biomolecules*, 10, 132.

Langer, F., Eisele, Y. S., Fritschi, S. K., Staufenbiel, M., Walker, L. C., & Jucker, M. (2011). Soluble Aβ seeds are potent inducers of cerebral β-amyloid deposition. *Journal of Neuroscience*, 31, 14488–14495.

Linse, S. (2019). Mechanism of amyloid protein aggregation and the role of inhibitors. *Pure and Applied Chemistry*, 91, 211–229.

Lu, J. X., Qiang, W., Yau, W. M., Schwieters, C. D., Meredith, S. C., & Tycko, R. (2013). Molecular structure of β-amyloid fibrils in Alzheimer's disease brain tissue. *Cell*, 154, 1257–1268.

Matsumura, S., Shinoda, K., Yamada, M., Yokojima, S., Inoue, M., Ohnishi, T., Shimada, T., Kikuchi, K., Masui, D., Hashimoto, S., Sato, M., Ito, A., Akioka, M., Takagi, S., Nakamura, Y., Nemoto, K., Hasegawa, Y., Takamoto, H., Inoue, H., ... Hoshi, M. (2011). Two distinct amyloid beta-protein (Abeta) assembly pathways leading to oligomers and fibrils identified by combined fluorescence correlation spectroscopy, morphology, and toxicity analyses. *Journal of Biological Chemistry*, 286, 11555–11562.

Meyer-Luehmann, M., Coomaraswamy, J., Bolmont, T., Kaeser, S., Schaefer, C., Kilger, E., Neuenschwander, A., Abramowski, D., Freym, P., Jaton, A. L., Vigouret, J. M., Paganetti, P., Walsh, D. M., Mathews, P. M., Ghiso, J., Staufenbiel, M., Walker, L. C., & Jucker, M. (2006). Exogenous induction of cerebral beta-amyloidogenesis is governed by agent and host. *Science*, 313, 1781–1784.

Morimoto, A., Irie, K., Murakami, K., Masuda, Y., Ohigashi, H., Nagao, M., Fukuda, H., Shimizu, T., & Shirasawa, T. (2004). Analysis of the secondary structure of beta-amyloid (Abeta42) fibrils by

systematic proline replacement. *Journal of Biological Chemistry*, 279, 52781–52788.

Murphy, R. G. L., Scanga, J. A., Powers, B. E., Pilon, J. L., Vercauteren, K. C., Nash, P. B., Smith, G. C., & Belk, K. E. (2009). Alkaline hydrolysis of mouse-adapted scrapie for inactivation and disposal of prion-positive material. *Journal of Animal Science*, 87, 1787–1793.

Nakayama, Y., Mineharu, Y., Arawaka, Y., Nishida, S., Tsuji, H., Miyake, H., Yamaguchi, M., Minamiguchi, S., Takagi, Y., & Miyamoto, S. (2017). Cerebral amyloid angiopathy in a young man with a history of traumatic brain injury: A case report and review of the literature. *Acta Neurochirurgica (wien)*, 159, 15–18.

Nguyen, P. H., & Derreumaux, P. (2020). Structures of the intrinsically disordered Aβ, tau and α-synuclein proteins in aqueous solution from computer simulations. *Biophysical Chemistry*, 264, 106421.

Nguyen, P. H., Ramamoorthy, A., Sahoo, B. R., Zheng, J., Faller, P., Straub, J. E., Dominguez, L., Shea, J. E., Dokholyan, N. V., De Simone, A., Ma, B., Nussinov, R., Najafi, S., Ngo, S. T., Loquet, A., Chiricotto, M., Ganguly, P., McCarty, J., Li, M. S., ... Derreumaux, P. (2021). Amyloid oligomers: A joint experimental/computational perspective on Alzheimer's disease, Parkinson's disease, type II diabetes, and amyotrophic lateral sclerosis. *Chemical Reviews*, 121, 2545–2647.

Ono, K., Condron, M. M., & Teplow, D. B. (2010). Effects of the English (H6R) and Tottori (D7N) familial Alzheimer disease mutations on amyloid beta-protein assembly and toxicity. *Journal of Biological Chemistry*, 285, 23186–23197.

Ono, K., Takahashi, R., Ikeda, T., & Yamada, M. (2012). Cross-seeding effects of amyloid β-protein and α-synuclein. *Journal of Neurochemistry*, 122, 883–890.

Ono, K., Takasaki, J., Takahashi, R., Ikeda, T., & Yamada, M. (2013). Effects of antiparkinsonian agents on β-amyloid and α-synuclein oligomer formation in vitro. *Journal of Neuroscience Research*, 91, 1371–1381.

Ono, K., & Tsuji, M. (2020). Protofibrils of amyloid-β are important targets of a disease-modifying approach for Alzheimer's disease. *International Journal of Molecular Sciences*, 21, 952.

Ono, K., Yoshiike, Y., Takashima, A., Hasegawa, K., Naiki, H., & Yamada, M. (2003). Potent anti-amyloidogenic and fibril-destabilizing effects of polyphenols in vitro: Implications for the prevention and therapeutics of Alzheimer's disease. *Journal of Neurochemistry*, 87, 172–181.

Penke, N., Bogár, F., & Fülöp, L. (2017). β-amyloid and the pathomechanisms of Alzheimer's disease: A comprehensive view. *Molecules*, 22, 1692.

Pietzke, M., Meiser, J., & Vazquez, A. (2020). Formate metabolism in health and disease. *Molecular Metabolism*, 33, 23–37.

Preusser, M., Ströbel, T., Gelpi, E., Eiler, M., Broessner, G., Schmutzhard, E., & Budka, H. (2006). Alzheimer-type neuropathology in a 28 year old patient with iatrogenic Creutzfeldt-Jakob disease after dural grafting. *Journal of Neurology, Neurosurgery and Psychiatry*, 77, 413–416.

Purro, S. A., Farrow, M. A., Linehan, J., Nazari, T., Thomas, D. X., Chen, Z., Mengel, D., Saito, T., Saido, T., Rudge, P., Brandner, S., Walsh, D. M., & Collinge, J. (2018). Transmission of amyloid-β protein pathology from cadaveric pituitary growth hormone. *Nature*, 564, 415–419.

Purrucker, J. C., Hund, E., Ringleb, P. A., Hartmann, C., Rohde, S., Schönland, S., & Steiner, T. (2013). Cerebral amyloid angiopathy–an underdiagnosed entity in younger adults with lobar intracerebral hemorrhage? *Amyloid*, 20, 45–47.

Raposo, N., Planton, M., Siegfried, A., Calviere, L., Payoux, P., Albucher, J. F., Viguier, A., Delisle, M. B., Uro-Coste, E., Chollet, F., Bonneville, F., Olivot, J. M., & Pariente, J. (2020). Amyloid-β transmission through cardiac surgery using cadaveric dura mater patch. *Journal of Neurology, Neurosurgery and Psychiatry*, 91, 440–441.

Ritchie, D. L., Adlard, P., Peden, A. H., Lowrie, S., Grice, M. L., Burns, K., Jackson, R. J., Yull, H., Keogh, M. J., Wei, W., Chinnery, P. F., Head, M. W., & Ironside, J. W. (2017). Amyloid-β accumulation in the CNS in human growth hormone recipients in the UK. *Acta Neuropathologica*, 134, 221–240.

Roychaudhuri, R., Yang, M., Hoshi, M. M., & Teplow, D. B. (2009). Amyloid beta-protein assembly and Alzheimer disease. *Journal of Biological Chemistry*, 284, 4749–4753.

Rudajev, V., & Novotny, J. (2020). The role of lipid environment in ganglioside GM1-induced amyloid β aggregation. *Membranes, (Basel)*, 10, 226.

Sahoo, B. R., Cox, S. J., & Ramamoorthy, A. (2020). High-resolution probing of early events in amyloid-β aggregation related to Alzheimer's disease. *Chemical Communications (Cambridge, England)*, 56, 4627–4639.

Sahoo, B. R., Genjo, T., Nakayama, T. W., Stoddard, A. K., Ando, T., Yasuhara, K., Fierke, C. A., & Ramamoorthy, A. (2019). A cationic polymethacrylate-copolymer acts as an agonist for β-amyloid and an antagonist for amylin fibrillation. *Chemical Science*, 10, 3976–3986.

Said, M. S., Navale, G. R., Yadav, A., Khonde, N., Shinde, S. S., & Jha, A. (2020). Effect of tert-alcohol functional imidazolium salts on oligomerization and fibrillization of amyloid β (1–42) peptide. *Biophysical Chemistry*, 267, 106480.

Sakudo, A. (2020). Inactivation methods for prions. *Current Issues in Molecular Biology*, 36, 23–32.

Sakudo, A., Higa, M., Maeda, K., Shimizu, N., Imanishi, Y., & Shintani, H. (2013). Sterilization mechanism of nitrogen gas plasma: Induction of secondary structural change in protein. *Microbiology and Immunology*, 57, 536–542.

Scheidt, T., Łapińska, U., Kumita, J. R., Whiten, D. R., Klenerman, D., Wilson, M. R., Cohen, S. I. A., Linse, S., Vendruscolo, M., Dobson, C. M., Knowles, T. P. J., & Arosio, P. (2019). Secondary nucleation and elongation occur at different sites on Alzheimer's amyloid-β aggregates. *Science Advances*, 5, 3112.

Schützmann, M. P., Hasecke, F., Bachmann, S., Zielinski, M., Hänsch, S., Schröder, G. F., Zempel, H., & Hoyer, W. (2021). Endo-lysosomal Aβ concentration and pH trigger formation of Aβ oligomers that potently induce Tau missorting. *Nature Communications*, 12, 4634.

Sciacca, M. F., Lolicato, F., Tempra, C., Scollo, F., Sahoo, B. R., Watson, M. D., García-Viñuales, S., Milardi, D., Raudino, A., Lee, J. C., Ramamoorthy, A., & La Rosa, C. (2020). Lipid-chaperone hypothesis: A common molecular mechanism of membrane disruption by intrinsically disordered proteins. *Current Issues in Molecular Biology*, 11, 4336–4350.

Simpson, D. A., Masters, C. L., Ohlrich, G., Purdie, G., Stuart, G., & Tannenberg, A. E. (1996). Iatrogenic Creutzfeldt-Jakob disease and its neurosurgical implications. *Journal of Clinical Neuroscience*, 3, 118–123.

Soto, C., & Pritzkow, S. (2018). Protein misfolding, aggregation, and conformational strains in neurodegenerative diseases. *Nature Neuroscience*, 21, 1332–1340.

Srivastava, A. K., Pittman, J. M., Zerweck, J., Venkata, B. S., Moore, P. C., Sachleben, J. R., & Meredith, S. C. (2019). β-Amyloid aggregation and heterogeneous nucleation. *Protein Science*, 28, 1567–1581.

Tarutani, A., Arai, T., Murayama, S., Hisanaga, S. I., & Hasegawa, M. (2018). Potent prion-like behaviors of pathogenic α-synuclein and evaluation of inactivation methods. *Acta Neuropathologica Communications*, 6, 29.

Thomzig, A., Wagenfuhr, K., Daus, M. L., Joncic, M., Schulz-Schaeffer, W. J., Thanheiser, M., Mielke, M., & Beekes, M. (2014). Decontamination of medical devices from pathological amyloid-beta-, tau- and alpha-synuclein aggregates. *Acta Neuropathologica Communications*, 2, 151.

Tiwari, S., Atluri, V., Kaushik, A., Yndart, A., & Nair, M. (2019). Alzheimer's disease: Pathogenesis, diagnostics, and therapeutics. *International Journal of Nanomedicine*, 14, 5541–5554.

Törnquist, M., Michaels, T. C. T., Sanagavarapu, K., Yang, X., Meisl, G., Cohen, S. I. A., Knowles, T. P. J., & Linse, S. (2018). Secondary nucleation in amyloid formation. *Chemical Communications (Cambridge, England)*, 54, 8667–8684.

Uchihashi, T., Kodera, N., & Ando, T. (2012). Guide to video recording of structure dynamics and dynamic processes of proteins by high-speed atomic force microscopy. *Nature Protocols*, 7, 1193–1206.

Watanabe-Nakayama, T., Ono, K., Itami, M., Takahashi, R., Teplow, D. B., & Yamada, M. (2016). High-speed atomic force microscopy reveals structural dynamics of amyloid β1-42 aggregates. *Proceedings of the National Academy of Sciences of the United States of America*, 113, 5835–5840.

Watanabe-Nakayama, T., Sahoo, B. R., Ramamoorthy, A., & Ono, K. (2020). High-speed atomic force microscopy reveals the structural dynamics of the amyloid-β and amylin aggregation pathways. *International Journal of Molecular Sciences*, 21, 4287.

Watts, J. C., Giles, K., Grillo, S. K., Lemus, A., DeArmond, S. J., & Prusiner, S. B. (2011). Bioluminescence imaging of Abeta deposition in bigenic mouse models of Alzheimer's disease. *Proceedings of the National Academy of Sciences of the United States of America*, 108, 2528–2533.

Watts, J. C., & Prusiner, S. B. (2018). β-Amyloid prions and the pathobiology of Alzheimer's disease. *Cold Spring Harbor Perspectives in Medicine*, 8, a023507.

WHO Infection control guidelines for transmissible spongiform encephalopathies. World Health Organization Report 23–26 March 1999, WHO/CDS/CSR/APH/2000.3, 1999.

Xue, W. F., Hellewell, A. L., Gosal, W. S., Homans, S. W., Hewitt, E. W., & Radford, S. E. (2009). Fibril fragmentation enhances amyloid cytotoxicity. *Journal of Biological Chemistry*, 284, 34272–34282.

Yamada, M., Hamaguchi, T., & Sakai, K. (2019). Acquired cerebral amyloid angiopathy: An emerging concept. *Progress in Molecular Biology and Translational Science*, 168, 85–95.

Yoo, J. H. (2018). Review of disinfection and sterilization—back to the basics. *Infection & Chemotherapy*, 50, 101–109.

Yoshiki, K., Hirose, G., Kumahashi, K., Kohda, Y., Ido, K., Shioya, A., Misaki, K., & Kasuga, K. (2021). Follow-up study of a patient with early onset cerebral amyloid angiopathy following childhood cadaveric dural graft. *Acta Neurochirurgica (wien)*, 163, 1451–1455.

Zhang, X., Xu, L., Huang, X., Wei, S., & Zhai, M. (2012). Structural study and preliminary biological evaluation on the collagen hydrogel crosslinked by γ-irradiation. *Journal of Biomedical Materials Research*, 100, 2960–2969.